NTNU
Norwegian University of
Science and Technology

The Effect of Low Temperatures on Energy Dissipation in Accidental Collisions on Marine Structures

Andreas Trollvik

Marine Technology
Submission date: June 2017
Supervisor: Jørgen Amdahl, IMT

Norwegian University of Science and Technology
Department of Marine Technology

MASTER THESIS 2017

For

Stud. Techn. Andreas Trollvik

The Effect of Low Temperatures on Energy Dissipation in Accidental Collisions on Marine Structures

Effekten av lave temperaturer på energidissipasjon ved kollosjoner på marine strukturer

Background

Floating offshore structures can be designed according to Recognized Class Societies rules like DNV GL or following the offshore design regime like ISO 19904-1 "Floating offshore structures". One of the challenges between these two approaches is how temperature is defined and the corresponding material selection. The common design standards for offshore structures set different requirements to how design temperature should be defined which are both confusing and can lead to very different requirements when it comes to selection of steel by using either the Class approach or the offshore approach. ISO 19906 for Arctic offshore structure defines the lowest anticipated service temperature (LAST) as the minimum hourly average temperature with a return period of 100 years, and recommends using LAST value for material selection. On the other hand, "Recognized Class Societies" (RCS) define the temperature to be used for material selection based on the Mean Daily Average Temperature (MDAT).

It is a known phenomenon that the steel in general becomes more brittle as the temperature decreases while the yield and tensile strength increase as the temperature gets colder. The latter effect is not accounted for in design standards today. The ice and icebergs texture and hardness are affected by different temperatures and gets harder and more brittle as the temperature drops.

Objectives of the work

- On a higher level discuss hull design for arctic floaters with comparison of the DNV GL rules and ISO 19904-1 from a design perspective.
- Compare the two design regimes for a site specific temperature of -10°C and -40°C when it comes to selection of steel material assuming the LAST regime in ISO 19904-1 and the MDAT for the recognized class society

The following topics should be addressed in the project work:

1. Review of rule requirements for hull design for Arctic conditions with focus material properties and qualities for low temperatures.
2. Literature review of stress-strain relationships for various steel materials steel as a function of (low) temperatures. Describe the relevant standard tests (e.g. Charpy V test, nil-ductility transition temperature test) to characterize the

properties at low temperatures. Discuss possible explanations why brittle fracture may occur, and describe briefly calculation models that have been proposed. Provide a brief review of large-scale tests that may be relevant.

3. Investigate the possibility of modelling ice behaviour with available material models in Abaqus. If feasible conduct iceberg impact with a rigid wall. Compare pressure-area relationships with relevant design curves.

4. For large scale simulations of accidents under Arctic or cryogenic conditions macro modelling brittle fracture is needed. Give a brief review of the model proposed by Woongshik Nam.

5. Simulate the impact tests at low temperatures conducted by Kim et. al. Int. Journal of Impact Engineering 93 (2016) 99âĂŞ115 and compare simulated response with laboratory measurements.

6. Establish a model for ABAQUS analysis of the side panel in the bow area of a large passenger vessel classed for 1A ice conditions with DNV-GL. Investigate the response with special attention on ductility assuming bergy-bit or ice-floe impact. If feasible, the ice may be included in the mechanical model, alternatively, ice pressure histories may be established fro varying contact area. Compare resistance curves obtained with Abaqus with hand calculations. Key parameters for steel material shall be varied. Conduct simple considerations regarding the probability of failure during design ice conditions.

7. Conclusions and recommendations for further work

Literature studies of specific topics relevant to the thesis work may be included.

The work scope may prove to be larger than initially anticipated. Subject to approval from the supervisor, topics may be deleted from the list above or reduced in extent.

In the thesis the candidate shall present his personal contribution to the resolution of problems within the scope of the thesis work.

Theories and conclusions should be based on mathematical derivations and/or logic reasoning identifying the various steps in the deduction.

The candidate should utilise the existing possibilities for obtaining relevant literature. The thesis should be organised in a rational manner to give a clear exposition of results, assessments, and conclusions. The text should be brief and to the point, with a clear language. Telegraphic language should be avoided.

The thesis shall contain the following elements: A text defining the scope, preface, list of contents, summary, main body of thesis, conclusions with recommendations

for further work, list of symbols and acronyms, references and (optional) appendices. All figures, tables and equations shall be numerated.

The supervisor may require that the candidate, in an early stage of the work, presents a written plan for the completion of the work. The plan should include a budget for the use of computer and laboratory resources, which will be charged to the department. Overruns shall be reported to the supervisor.

The original contribution of the candidate and material taken from other sources shall be clearly defined. Work from other sources shall be properly referenced using an acknowledged referencing system.

The report shall be submitted in two copies:

- Signed by the candidate
- The text defining the scope included
- In bound volume(s)
- Drawings and/or computer prints which cannot be bound should be organised in a separate folder.

Supervisor:

Prof. Jørgen Amdahl

Contact persons at MTS:
Ph.D.-student Woongshik Nam,
Postdoc Ekaterina Kim

Supervisor DNV GL:
Erling Østby

Deadline:, June 10 2017

Trondheim, January 11, 2017

Jørgen Amdahl

Abstract

The effect of low temperatures on impacts between ships and icebergs have been investigated. A material model developed by Woongshik Nam has been used for modelling the effect of brittle fracture. To test the model, an experimental study done by Kim et al (2016) has been replicated in Abaqus. After the impact study was replicated, an impact between the fore part of a DNVGL ICE-1A classed vessel and a circular ice body was simulated. As no material model for ice was found for Abaqus, the ice body was modelled as a rigid disc with a diameter of 10 meter and a thickness of 1.2 meter. The ship model was supplied by Suyu Wang and the Nam (2017) material model was used for the steel. The impact was simulated at a range of different temperatures, ranging from room temperature to -100°C. For the impact, the ice body was given an initial velocity of 0.5 m/s and had a mass of 1000 tonnes. Each simulation was run for 0.5 s.

The Kim et al (2016) study was an impact test of two panels, one stiffened and one unstiffened. These panels were impacted by a striker at two temperatures, room temperature and -60°C. In Abaqus the experiments were modelled with FEM by using both normal material parameters and the material code supplied by Woongshik Nam. The analysis showed that the Nam material model gave good results for the stiffened panel, compared to both the normal material and the experimental results. For the unstiffened panel, it was discovered that the bending stiffness of the two material codes was different. However, as the ship side is stiffened in both longitudinal and transverse direction, this should not influence the result.

The studies of the ship side showed a correlation between the temperature and the damage of the ship. As temperatures lowered, the damage of the ship side became more severe. With lower temperature, the collision energy was dissipated slower by the ship side. At the lowest temperature, -100°C, only 38% of the total energy had been absorbed by the end of the simulation and the ship side had severe damage.

The failure criteria for temperatures between -60°C and -100°C has been interpolated from predefined failure criteria at -60°C, -100°C and -140°C. This leads to some uncertainties regarding the results at the intermediate temperatures. Some problems have been found with the ship side model. Two areas of the model have areas where elements from stiffener and bulkheads overlap, which creates some artificial stresses. In addition, some stress hot spots are created by the mesh. However, these areas are not close to the impact zone, and is not believed to have effected the results.

Overall, the results from the analysis displays the dangers of low temperatures in accidental impacts. The effect of the embrittlement of steel is reflected in the analysis, and should be taken into account when designing vessels for Arctic environments. However, further studies of the topic are needed before a clear conclusion can be drawn.

Sammendrag

Effekten av lave temperaturer på sammenstøt mellom skip og isfjell har blitt undersøkt. For å modellere effekten av forsprøing av stål har en materialmodell utviklet av Woongshik Nam (2017) blitt brukt, for verifikasjon av materialmodellen har en eksperimentell studie utført av Kim et al (2016) blitt replisert i Abaqus. Etter kollisjonsstudien ble et sammenstøt mellom den fremre delen av et DNV GL ICE-1A klasset fartøy og et sirkulært islegeme simulert. Islegemet ble modellert som et ubøyelig skive med en diameter på 10 meter og en tykkelse på 1.2 meter. Skipsmodellen ble laget av Suyu Wang og materialkoden utviklet av Woongshik Nam ble brukt. Sammenstøtet ble simulert over en rekke temperaturer, fra romtemperatur til -100°C, islegemet ble gitt en initial hastighet på 6 m/s og hadde en masse på 1000 tonn. Hver analyse ble kjørt over et tidsrom på 0.5 s.

Kim et al (2016) studien var en kollisjonsstudie utført på to paneler, et avstivet og et ustivet. Disse panelene ble utsatt for en kollisjon ved romtemperatur og -60°C. Dette eksperimentet ble gjenskapt i Abaqus og utført ved bruk av en normal materialmodell og materialmodellen utviklet av Nam. Analysen viste at Nams materialmodell ga gode resultater for det avstivede panelet, både sammenlignet med den normale materialmodellen og med det eksperimentelle resultatet. For panelet uten stivere ble det oppdaget at det var en forskjell i bøyestivheten for de to materialmodellene. Siden skipssiden er modellert med stivere både i tverrgående og langsgående retning, skal ikke dette påvirke resultatet av skipsside-analysen nevneverdig.

Analysen av skipssiden viste en korrelasjon mellom temperaturen og skaden på skipssiden. Når temperaturen sank, ble skadene på skipssiden verre. Ved lave temperaturer tok det lengre tid før kollisjonsenergien var absorbert av skipssiden. På den laveste temperaturen, -100°C, var bare 38% av kollisjonsenergien absorbert ved slutten av analysen, og skipssiden hadde allerede fått alvorlige skader.

Sviktkriteriet for temperaturene mellom -60°C og -100°C har blitt interpolert fra definerte sviktkriterier ved -60°C, -100°C og -140°C. Dette medfører noe usikkerhet knyttet til resultatet ved disse mellomliggende temperaturene. I tillegg har noen problemer med skrogmodellen blitt indentifisert. I to områder av modellen fører overlapp mellom elementer i stivere og i skott til kunstige spenninger. Videre har meshingen av elementene ført til at noen spenningskonsentrasjoner oppstår. Ingen av disse områdene er i nærheten av kollisjonssonen, så det er ikke trodd at dette påvirker resultatet.

Alt i alt viser analysene hvilken fare lave temperaturer utgjør i kollisjoner. Effekten av forsprøing av stål er gjenspeilet i resultatene fra analysene og burde tas hensyn til når fartøy for bruk i arktiske miljøer blir designet. Det trenges derimot videre studier av temaet før en sikker konklusjon kan trekkes.

Preface

This master thesis was written during the spring of 2017 at the Norwegian University of Science and Technology, at the institute of marine technology. The thesis is completed with the cooperation of DNV GL.

I wish to thank Jørgen Amdahl for his role as supervisor at the university and guidance during the thesis. His input and help on the thesis material has been critical for the completion of the thesis. Thanks to Woongshik Nam for his role as co-supervisor and for the possibility to use his code. Without his help in troubleshooting Abaqus and the Fortran compiler this thesis would not have been completed. Thanks to Ekaterina Kim for her role as co-supervisor and help on the topic of ice models.

A special thanks to Suyu Wang for supplying me with the ship side model. I am painstakingly aware of the amount of time spent on creating the model, and am deeply grateful for the possibility of using the model.

Last but not the least, a grand thank to all of my friends, family and classmates for support, feedback and constructive questions. I would have been at a loss without the possibility to ask questions and test ideas and theories with you.

Andreas Trollvik

Table of Contents

List of Tables

List of Figures

Abbreviations

ALS	=	Accidental limit state
BCC	=	Body centered cubic
BV	=	Bureau Veritas
BWH	=	Bressan, Williams and Hill
CVN	=	Charpy-V notch
DAT	=	Design ambient temperature
DBFT	=	Ductile to brittle fracture transition
DBTT	=	Ductile to brittle transition temperature
DNV	=	Det Norske Veritas
FE	=	Finite element
FEA	=	Finite element analysis
FEM	=	Finite element method
GL	=	Germanischer Lloyd
HAZ	=	Heat affected zone
IACS	=	International Association of Classification Societies
IMO	=	International Maritime Organization
ISSC	=	International Ship and Offshore Structures Congress
LAST	=	Lowest anticipated service temperature
LMDAT	=	Lowest mean daily average temperature
LNG	=	Liquid natural gas
LOA	=	Length overall
LPP	=	Length between perpendiculars
LR	=	Lloyd's Register
RCS	=	Recognized class societies
RP	=	Recommended practice
SED	=	Strain energy density
SZT	=	Sub-zero temperature
ULS	=	Ultimate limit state

Chapter 1

Introduction

DNV GL expects about 480 annual trans-arctic voyages for container ships by the year 2030 [DNVGL (2010)]. For ships sailing in the Arctic, sub-zero temperatures will be a frequent occurrence. Several classification societies have rules and recommendations which takes ice actions into account, however the effect of sub-zero temperatures is not taken into account by these rules.

The effect of temperature on the brittleness of steel is not accounted for in design standards today. Understanding the effect of low temperatures has on damage after accidental impact will be important for designing safe and cost effective vessels for use in the Arctic. This thesis will do an initial investigation into the effect of low temperature and on how it might effect the damage after an accidental impact.

Woongshik Nam is currently working on a material model for large scale shell elements which takes brittle fracture of the material into account by combining the extended BWH criterion proposed by Storheim and the plastic strain energy criterion. This material model will be used to investigate for brittle fracture in a ship-iceberg collision.

1.1 Problem Description

By using the FEM-program Abaqus, an iceberg impact with a ship side is analysed. In addition, the material model is tested by replicating an impact study carried out by Kim et al (2016) A study of rules and standards regarding steel structures in polar environments will provide some data for comparison with the results from the FEM-analysis.

1.2 Outline

This thesis is divided into 7 chapters; introduction, background material, rule requirements, finite element analysis, results, discussion and conclusion. Chapter 2

provides theory on brittle fracture, the temperature effect on steel, FE models for modelling ice and non-linear finite element methods. Chapter 3 contains a review of rules and standards regarding steel structures in Arctic climate. Chapter 4 gives information on the models used for the FEM-analysis of both the Kim et al (2016) drop test and the ship side impact. Chapter 5 presents the results of these analyses and some discussion of the results. A general discussion of the results will be carried out in Chapter 6. The final chapter presents a conclusion and recommendations for further work.

Chapter 2

Background Material

This chapter provides necessary background material for the rest of the content. Non-linear finite element methods will be discussed, along with theory on material properties. In addition, some ice models for FEA will be described.

2.1 Brittle Fracture

It is a known phenomenon that the material properties of metallic materials with a body-centred cubic (BCC) structure, such as steel, changes with temperature. As the temperature lowers, the material turns more brittle and fracture becomes an issue. This transition is called the ductile to brittle temperature, DBTT. The DBTT is highly dependant upon the composition of the metal. Highly pure iron without any carbon and nitrogen maintains its ductility at very low temperatures [Bhadeshia and Honeycombe (2006)].

It is worth noting that no explicit criterion is defined for the DBTT, which leads to different studies using different criteria for DBTT.

For a floater operating in Arctic conditions this will be a major issue, since the ambient temperature might enter the ductile to brittle transition temperature range. Due to this, brittle fracture should be taken into account for ships and structures in Arctic environments [Nam and Amdahl (2016)]. When operating in sub-zero temperatures, SZT, special materials might be needed. Most steels designed for SZT typically shows an increase in ultimate strength, yield strength and Lüders plateau length, while having a decrease in fracture strain with decreasing temperature [Ehlers and Ostby (2012)]. The Arctic material will show an increase in load capacity until the point of fracture. If the fracture strain of the Arctic material can be increased, the total load carrying capacity will be increased. Ehlers and Østby (2012) tested the difference in penetration of an impact at SZT when using a normal NVA steel and an Arctic steel and states that a gain of 30 % in collision force prior to rupture can be achieved by choosing a suitable material.

2.2 Property Testing

In general, two types of tests are done to characterize the elastic properties of a material, tensile tests and impact tests. A tensile test is carried out by stretching a specimen of the material, while measuring the elongation and the force. These tests are standardized by ASTM E8/E8M and ISO 6892. To avoid any strain-rate effects, these tests are normally carried out quasi-static.

Impact tests are tests which are done to ascertain the fracture properties of materials at high loading rates. These are done as the results from laboratory testing at low load rates can not be extrapolated to high rates [Callister and Rethwisch (2011)]. Two standardized tests for measuring the impact energy are the Charpy-V and the Izod test. Both these tests uses the same test geometry, the primary difference is in the support of the specimen.

The CVN-test is done on a bar with a square cross section, which has a v-shaped notch machined in it. The bar is then impacted with a hammer on a pendulum, which is released from a known height. After impact, the height at the end of the swing is measured. The energy expended in the fracture can then be calculated from the difference in the initial height and the end height. To check for a DBTT, the CVN-test is repeated at incrementally lower temperature and the impact energy is plotted against the temperature. It is worth noting that the result from an impact test is mostly qualitative and have little use for design purposes.

2.3 Materials for Sub-zero Temperatures

In 2011 Søren Ehlers and Erling Østby published a study on the effect on crashworthiness of using materials designed for low temperatures. In this study, they compared the force-indentation curves of a simulated impact using both normal steel and low temperature steel. The simulation was carried out at -30°C, -60°C and -90°C. In addition, it was compared to a large scale collision experiment carried out during the EU Crashcoaster project. In their study, they found that using a material designed for low temperatures could lead to a 30% increase in the maximum allowed collision force [Ehlers and Ostby (2012)].

2.4 Modelling of Brittle Fracture

Several criteria have been made to model brittle fracture. This section will briefly describe some of these.

2.4.1 BWH-criterion

The BWH-criterion is a combination of the local necking analysis done by Hill in 1952 and the shear stress criterion developed by Bressan and Williams. The BWH-criterion is dependant upon the stress rate ratio, β, which is defined as given in Equation (2.1).

$$\beta = \frac{\dot{\epsilon_2}}{\dot{\epsilon_1}} = \frac{2\alpha - 1}{2 - \alpha}, \alpha = \frac{\sigma_2}{\sigma_1} \tag{2.1}$$

The BWH criteria gives the critical stress as given in Equation (2.2) .

$$\sigma_1 = \begin{cases} \frac{2K}{\sqrt{3}} \frac{1+\frac{1}{2}\beta}{\sqrt{\beta^2+\beta+1}} \left(\frac{2}{\sqrt{3}} \frac{\hat{\epsilon}_1}{1+\beta} \sqrt{\beta^2+\beta+1} \right)^n, & \text{if } -1 < \beta \leq 0. \\ \frac{2K}{\sqrt{3}} \frac{\left(\frac{2}{\sqrt{3}}\hat{\epsilon}_1\right)^n}{\sqrt{1-(\frac{\beta}{2+\beta})^2}} & \text{if } 0 < \beta \leq 1. \end{cases} \tag{2.2}$$

In Equation (2.2) K and n are the hardening parameters, and $\hat{\epsilon}_1$ is the critical strain and can be set to be equal to n [Storheim (2015)]. However it was reported by Alsos et al (2009) that using measured values of $\hat{\epsilon}_1$ gives better correlation with experimental results in some cases.

2.4.2 Woongshik Nam Model

A phd candidate at NTNU's department of Marine Technology, Woongshik Nam is currently working on a material model combining the extended BWH criterion and the plastic strain energy criterion to predict the ductile to brittle fracture transition, DBFT. This model is currently under development and will be tested in this thesis. This model is an extension of the extended BWH criterion proposed by Martin Storheim in his doctoral thesis. The model proposed by Storheim is based on the J2 flow theory, i.e von Mises yield criterion. It defines a scalar damage variable, D, which is zero when the element is undamaged and unity for a fully damaged shell element. D is defined as given in Equation (2.3), where β is as defined in Section 2.4.1, $\Delta\epsilon_1$ is the normal strain of the element in the direction perpendicular to the local neck ad t_0 and l_0 is the initial thickness and length of the element [Storheim (2015)].

$$D = \begin{cases} 1 - \frac{exp((1+\beta)\Delta\epsilon_1}{1+\frac{l_0}{t_0}[exp((1+\beta)\Delta\epsilon_1)-1]} & \text{if } -1 < \beta \leq 0 \\ 1 - \frac{exp(\Delta\epsilon_1)}{1+\frac{l_0}{t_0}[exp(\Delta\epsilon_1)-1]} & \text{if } 0 \leq \beta \leq 1 \end{cases} \tag{2.3}$$

When necking occurs, the strength of the element will gradually be reduced. Storheim (2015) assumes the final fracture and thus the erosion of an element to be controlled by the total thickness strain within the virtual neck, $\tilde{\epsilon}_3$. Storheims erosion criterion is defined as given in Equation (2.4), where ξ and ψ are input material parameters to the model. For normal marine structural steels, ξ can be assumed to be 1. Assuming ψ to be close to unity is a conservative estimate, and Storheim (2015) assumes $\psi = 0.9$ in his thesis. Once $\tilde{\epsilon_3}$ reaches $\tilde{\epsilon_{3,max}}$ an integration point is assumed to fail. If the mid integration point through the thickness reaches critical strain, the element is eroded.

$$\tilde{\epsilon}_{3,max} \begin{cases} \epsilon_3^0(1+\xi) & \text{if } -1 < \beta \leq 0 \\ \epsilon_3^0(1+\xi(1-\psi\beta)) & \text{if } 0 < \beta \leq 1 \end{cases} \tag{2.4}$$

Wongshik Nams model combines Storheims criterion, as describe above, with the plastic strain energy density criterion. By combining these two criteria, the critical strain energy shows a consistent tendency upon β. As it is dependant upon the critical strain energy, different cases of initial crack shapes can easily be taken into account by changing the critical strain energy. In addition, the plastic strain energy density criterion is relatively independent upon the mesh size [Nam (2017)].

2.5 Ice Material Model

To model a shared energy approach impact, an ice model is required. Despite of this, there is no established ice model for Abaqus. A strain rate sensitive ice model was developed at the University of California, San Diego by Tippmann (2011), however this model is made to simulate hail impacts on air-planes. The model was based on simple elastic-plastic behaviour, with a tensile hydrostatic pressure based failure criterion. To accurately predict the impact force, the mesh in the hail is required to be less than 0.5 mm, which is too fine for use in a larger ice body. Due to the model being created for large strain rate hail impacts with strain rates above 10 s^{-1} it is not suitable for modelling the relative slow strain rate impact of a ship. Liu et al (2011) states that the strain rates in ship-iceberg impacts is found to be between $4 \cdot 10^{-3}s^{-1}$ to $4 \cdot 10^{-1}s^{-1}$, which is below the strain rates used by Tippmann. In addition, the young fresh water ice used to create Tippmanns model is not representative for old sea and iceberg ice.

Liu et al. (2011) developed a ice model for the FEA-program LS-DYNA, which uses the Tsai-Wu yield surface. The failure criteria is given in Equation (2.5) and Equation (2.6), where ϵ^p_{eq} is the equivalent plastic strain, ϵ_f is the failure yield, ϵ^p_{ij} is the plastic strain tensor, ϵ_0 is the initial failure strain and p_2 is the larger root of the yield function. Erosion of the element is activated if $\epsilon^p_{eq} > \epsilon_f$ or if the pressure is not larger than the cut-off pressure [Liu et al. (2011)]. This model was written to an Abaqus VUMAT by Ferrari (2014).

$$\epsilon^p_{eq} = \sqrt{\frac{2}{3}\epsilon^p_{ij} : \epsilon^p_{ij}} \tag{2.5}$$

$$\epsilon_f = \epsilon_0 + \left(\frac{p}{p_2} - 0.5\right)^2 \tag{2.6}$$

In addition, an ice model has been developed by Moore et al (2011). This model is based on Kachanovs work on damage mechanics, which defines a damage parameter, D, defined as given in Equation (2.7). Using this damage parameter, the effective stress can be written as in Equation (2.8).

$$D = \frac{A}{A_0}, 0 \leq D < 1 \tag{2.7}$$

$$\sigma_a = \frac{P}{A_0 - A} = \frac{\sigma}{1 - D} \tag{2.8}$$

In 1981 Schapery devised an unbounded damage parameter, which Moore et al. (2011) used to create their ice model. The damage parameter used is given in Equation (2.9), where S_1 relates to microcracking and is dominant at low confinement and S_2 relates to pressure melting, pressure softening and dynamic recrystallization and dominates at high confinement. In Equation (2.9), s is von Mises stress, σ_0 is reference stress, q_1 is the power law exponent, which is taken as 5 in Moore et als paper, and f_1 and f_2 is as defined in Equations (2.10) and (2.11), where p is pressure and r is a empirical constant.

$$S = S_1 + S_2 = \int_0^t \left(f_1(p)\left(\frac{s}{\sigma_0}\right)^{q_1} + f_2(p) exp\left(\frac{s}{\sigma_0}\right) \right) dt \tag{2.9}$$

$$f_1(p) = \begin{cases} 0.712\left(1 - \frac{p}{37}\right) & \text{if } p < 37\text{MPa} \\ 0 & \text{if } p \geq 37\text{MPa} \end{cases} \tag{2.10}$$

$$f_2(p) = 0.1\left(\frac{p}{42.8}\right)^r \tag{2.11}$$

The model uses a Kelvin-Maxwell model, see Figure 2.1, known as Burgers body representation, to model viscoelastic strain rate effects.

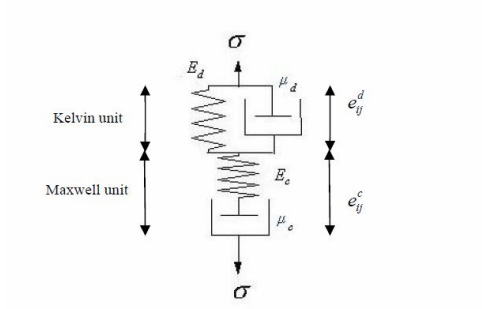

Figure 2.1: Burgers body representation of ice properties, courtesy to Moore et al. (2011).

However, none of the ice material models for Abaqus is publicly available and rewriting one of the existing ice material models for Abaqus is outside the scope of this thesis.

2.6 Solution Methods for Non-linear Problems

When solving finite element (FE) problems with large deformations, linear finite element methods can not be used. As deformations get large, the stress might leave the elastic zone and plastic deformations might occur. In addition, geometrical effects might make the construction stiffer. Due to these effects, most modern design codes allows for the use of nonlinear FE when checking for ALS and ULS.

Most solution methods for non-linear problems attempt to discretizate the continuous non-linear displacements by using a series of linearised increments of displacement. There are several different methods of doing this, the two most used methods in Abaqus will be shortly described in the following section.

2.6.1 Newton-Rapshon Method

The Newton-Rapshon Method is one of the most frequently used iterative method for solving non-linear FEM problems. It is based on a generalized version of Equation (2.12), where $f'(x)$ is the space derivative of f(x) with respect to x at $x = x_n$. In the following section, Δ will be used for the initial predictor change, while δ is used for iterative changes. For each step, the basic target is to find a solution to the energy balance, Equation (2.13).

$$x_{n+1} = x_n - \frac{f(x_n)}{f'(x_n)} \tag{2.12}$$

$$R^n_{ext} = R^n_{int} \tag{2.13}$$

The internal work of the structure, R^n_{int} might formally be written as shown in Equation (2.14). By defining the incremental stiffness matrix, K^n_{inc} as in Equation (2.15), the internal work for step $n+1$ might be expressed by Equation (2.16). This will for most iterations give an unbalanced force, as shown in Equation (2.17).

$$\begin{aligned} R^{n+1}_{int} &= R_{int}(r^n + \Delta r) \\ &\approx R_{int}(r^n) + \left.\frac{\delta R}{\delta r}\right|_{r=r^n} \Delta r \end{aligned} \tag{2.14}$$

$$K^n_{inc} = \left.\frac{\delta R}{\delta r}\right|_{r=r^n} \tag{2.15}$$

$$R^{n+1} = R^n + k^n_{inc}\Delta r \tag{2.16}$$

$$K^n_{inc}\Delta r = R^{n+1}_{ext} - R^n_{int} = R_{unb} \tag{2.17}$$

After the nodal degree of freedom, Δr, is solved from one of the above equations, the C^n configuration can be updated with respect to the following variables.

- Displacement vector, $r^{n+1} = r^n + \Delta r$
- Modal coordinates
- Element stresses and strains, $\sigma^{n+1} = \sigma^n + \Delta\sigma$

A new iteration starts after the C^n configuration have been updated, following the steps shown in Equation (2.18)

$$\begin{aligned} R_{int}^{n+1} &= R_{int}(r^{n+1} + \delta r) \\ &\approx R_{int}(r^{n+1}) + K_{inc}^{n+1}\delta r \\ K_{inc}^{n+1}\delta r &= R_{int}^{n+1} - R_{int}^{n+1} = R_{unb} \end{aligned} \tag{2.18}$$

After each iteration, the C^{n+1} configuration is updated with respect to the new displacement vector, $r_{new}^{n+1} = r_{old}^{n+1} + \delta r$, modal coordinates, element stresses etc. After updating, a check for equilibrium has to be carried out. The equilibrium check is usually taken as a norm of δr to be smaller than a prescribed value, as shown in Equation (2.19). Two commonly used formulations are the displacement requirements, shown in Equations (2.20) and (2.21). Other formulations, such as a force norm and energy norm may also be used. If the found δr is less than the prescribed value, the next step is carried out and a new Δr can be added, if not, more iterations is needed.

$$norm(\delta r) < \epsilon_r \tag{2.19}$$

$$norm(\delta r) < \frac{1}{r_{ref}}|\delta r|max \tag{2.20}$$

$$norm(\delta r) < \sqrt{\frac{1}{N}\sum_{i=1}^{N}\left(\frac{r_k}{r_{ref}}\right)^2} \tag{2.21}$$

2.6.2 Riks-Wempner Method

The Riks-Wempner method is a method used to calculate the displacements of a structure after the limit point, i.e. after the point of ultimate strength. This is done to be able to assess the failure mechanisms and the damage after failure of the structure. The Riks-Wempner method defines the global equilibrium as given in Equation (2.22), where R_{ref} is a fixed external load vector and λ is a load level parameter. The method then uses a linear, incremental method, the arc-length method, to solve the system. The arch length method is based on finding an equilibrium path in the r-λ plane, where λ is the loading parameter. The increment size is limited by moving a fixed distance along the tangent line for the current solution to a point and finding an equilibrium in the plane that passes through the point and is orthogonal to the tangent line.

$$g(r, \lambda) = R_{int}(r) - \lambda R_{ref} = 0 \tag{2.22}$$

In Abaqus, a modified Riks method is used, scaling the load-displacement space to ensure that the dimensions is of the same magnitude [Abaqus (2009)]. The actual load for each step is found using the displacement parameter and is given as

λP^N for step N. The displacements at time N is denoted u^N. The scaled space is then defined by load, $\lambda\tilde{P}^N$, where $\tilde{P}^N = \frac{P^N}{|P|}$ and the displacement is $\tilde{u}^N = \frac{u^n}{|u|}$.

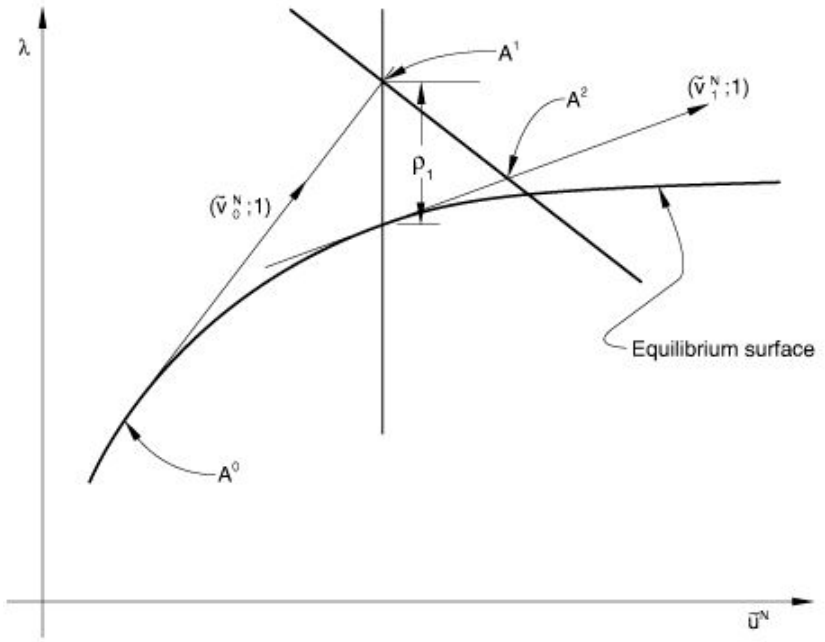

Figure 2.2: Illustration of the Riks method, courtecy to Abaqus (2009)

Figure 2.2 shows an illustration of the steps carried out. Assuming that the solution has been found to the point $A^0 = (\tilde{u}_0^N, \lambda_0)$. At this point, the tangent stiffness, K_0^{NM} is formed and the problem $K_0^{NM} v_0^M = P^N$ is solved. The increment size, the distance from A^0 to A^1 in Figure 2.2, is chosen such that the path length, Δl, in the solution space is as given in Equation (2.23).

$$\Delta\lambda_0^2(\tilde{v}_0^N;1) : (\tilde{v}_0^N;1) = \Delta l^2 \tag{2.23}$$

By rewriting Equation (2.23) one finds the loading parameter as a function of path length, as given in Equation (2.24).

$$\Delta\lambda_0 = \frac{\pm\Delta l}{(\tilde{v}_0^N \tilde{v}_0^N + 1)^{\frac{1}{2}}} \tag{2.24}$$

The solution is then corrected onto the equilibrium plane passing through A^1 and orthogonal to $(\tilde{v}_0^N;1)$ by the following iterative steps:

- Initialize by $\Delta\lambda_i = \Delta\lambda_0, \Delta u_i^N = \Delta\lambda_0 v_0^N$
- For each iteration i:

1. Find the internal forces at the nodes, I^N and the stiffness, K^{NM} at point A^i from:
$$I^N = \int_v \beta^N : \sigma dV$$
$$K^{NM} = \frac{\delta I^N}{\delta u^M}$$

2. Check equilibrium using:
$$R_i^N = (\lambda_0 + \Delta\lambda_i)P^N - I^N \tag{2.25}$$

3. If all entries in Equation (2.25) are small, the increment has converged. If not, solve Equation (2.26) for $v_i^N$and c_i^N.
$$K^{NM}(v_i^M; c_i^M) = (P^N; R_i^N) \tag{2.26}$$

4. Scale the $(\tilde{v}_i^N; 1)$-vector and add it to the $(\tilde{c}_i^N; p_i)$-vector, where $p_i = R_i^N \frac{P^N}{|P^2|}$, to move from A^i to A^{i+1} in the orthogonal plane. From this the solution point A^i is found to be $(u_0^N + \Delta u_i^N + c_i^N + \mu v_i^N; \lambda_0 + \Delta\lambda_i + \mu$, where μ is found as shown in Equation (2.27).
$$\mu = -\frac{\tilde{c}_i^N \tilde{v}_o^N}{\tilde{v}_i^N \tilde{v}_o^N + 1} \tag{2.27}$$

5. Update for next iteration and restart.
$$\Delta u_{i+1}^N = \Delta u_i^N + c_i^N + \mu v_i^N$$
$$\Delta\lambda_{i+1} = \Delta\lambda + \mu$$

2.6.3 Explicit Solution Methods

Explicit solution methods uses accelerations, velocities and displacements of previous time steps to find displacements at the next time step, $t+\Delta t$. There are several different explicit methods, one of them is the central difference method. The central difference method is based on the assumption that a taylor series expansion can be used to find the displacement at the next step, $t+\Delta t$, and the previous time step, $t-\Delta t$. This results in the expressions shown in Equations (2.28) and (2.29). By neglecting all terms with power of three and higher, the expression shown in Equation (2.30) can be found by subtraction.

$$r_{i+1} = r_0(t) + \Delta t\dot{r}_i + \frac{\Delta t^2}{2}\ddot{r}_i + \frac{\Delta t^3}{6}\dddot{r}_i + ... \tag{2.28}$$

$$r_{i-1} = r_0(t) - \Delta t\dot{r}_i + \frac{\Delta t^2}{2}\ddot{r}_i - \frac{\Delta t^3}{6}\dddot{r}_i + ... \tag{2.29}$$

$$r_{i+1} - r_{i-1} \approx 2\Delta t\dot{r}_i \tag{2.30}$$

Using the above equations, the velocities and accelerations at the current time step can be expressed as shown in Equations (2.31) and (2.32).

$$\dot{r_i} = \frac{1}{2\Delta t}(r_{i+1} - r_{i-1}) \tag{2.31}$$

$$\ddot{r_i} = \frac{1}{2\Delta t^2}(r_{i+1} - 2r_i(t) + r_{i-1}) \tag{2.32}$$

By inserting Equations (2.31) and (2.32) into the equation of motion, Equation (2.33), the expression in Equation (2.34) is found.

$$\mathbf{M}\ddot{r} + \mathbf{C}\dot{r} + \mathbf{K}r = \mathbf{R}_i(t) \tag{2.33}$$

$$\left(\frac{1}{\Delta t^2}\mathbf{M} + \frac{1}{2\Delta t}\mathbf{C}\right)r_{i+1} = \mathbf{R}_i(t) - \mathbf{K}r_i(t) + \frac{1}{\Delta t^2}\mathbf{M}(2r_i - r_{i-1}) + \frac{1}{2\Delta t}\mathbf{C}r_{i-1} \tag{2.34}$$

As long as the mass matrix, $\mathbf{M}$, and the damping matrix, $\mathbf{C}$, are diagonal, the equations will be uncoupled. If this is the case, the displacements at the next time step, $t + \Delta t$, can be found without solving simultaneous equations.
The explicit method has the advantage of being non-singular as long as the mass matrix is non-zero. In addition, there is no need to invert the tangent stiffness matrix at every time step. Since the method finds the internal force vector by summation of element contributions, the global stiffness vector does not need to be stored. This leads to a drastic reduction of required computer memory capacity.

Chapter 3

Rule Requirements

This chapter contains a review of rule requirements in hull design for Arctic conditions, with focus on plate thickness and material requirements. The main focus will be the difference in basis for the different rules and RPs.

3.1 General Design

Both ISO 19904 and RCS uses limit state design, in which the structure is designed to withstand a specified set of limit states. In this report, the ultimate limit state (ULS) and accidental limit state (ALS) will be discussed. For design, the number of design situations shall be chosen to ensure that all critical load combinations for all load bearing components of the structure is included [ISO (2006)].
The ULS is meant to ensure that the structure is able to withstand all normal loads and load combinations which is expected to happen. The loads shall be chosen with a return period of 10^{-2} years. ALS shall cover accidental and abnormal events, such as fire, rouge wave or impact. The return period for the ALS load is 10^{-4} years. In addition, the damage after an ALS event shall not affect the overall stability, integrity or safety of the structure.
The limit state principle is based on the design load effect, S_d, which shall not exceed the design resistance R_d. According to DNV GL (2015), a structure is satisfactory if:

$$S_d \leq R_d$$

3.1.1 Plate Thickness

The DNV GL Cold Climate rules are based on linear theory, using yield as a failure criteria [Amdahl (2015)]. The thickness criteria is derived from the bending stress, which is given in its most basic form in Equation (3.1). The bending stress is evaluated at the mid-point of the plate strip, even though the bending stress

is larger at the boundaries. However, the plate resistance will increase due to development of membrane stresses at the plate boundaries. This is probably the reason for evaluating the stresses at the mid span [Amdahl (2015)].

$$t = \frac{1}{2} s \sqrt{\frac{p}{\sigma}} \tag{3.1}$$

Due to section 3 and 4 of the Cold Climate rules having no specific requirements to plate thickness, the requirements from Pt. 6 Ch. 6, Section 2 - "Ice Strengthening for the northern Baltic" will be discussed in this section. The DNV GL Cold Climate Rules requires the plate thickness in the ice belt to be as in Equation (3.2) for plates with transverse frames and as in Equation (3.3) for plates with longitudinal frames.

$$t = 21.1 \cdot s_1 \sqrt{\frac{f_1 \cdot P_{PL}}{R_{eH}} + t_c} \tag{3.2}$$

$$t = 21.1 \cdot s_1 \sqrt{\frac{P}{f_2 \cdot R_{eH}} + t_c} \tag{3.3}$$

Where the following parameters are used:
$P_{PL} = 0.75P$
$P = 5600 \cdot c_d \cdot c_1 \cdot c_a$
c_d is a factor which takes the influence of engine size and power into account and can be found from section 7.3.1 in [DNVGL (2016)]
c_1 is a factor which takes the probability of the design ice pressure occurring in a certain region of the hull into account, can be found from section 7.3.1 in [DNVGL (2016)]
c_a is a factor which takes the probability that the full length of the area considered will be under pressure at the same time, calculated from $c_a = \sqrt{\frac{l_o}{l_a}}$, where l_a is found from section 7.3.1 in [DNVGL (2016)]
$f_1 = 1.3 - \frac{4.2}{(h/s_1+1.8)^2}$, maximum 1.0

$$\begin{aligned} f_2 &= 0.6 + \frac{0.4}{h/s_1} \text{ if } h/s_1 \leq 1 \\ &= 1.4 - 0.4 \cdot h/s \text{ if } 1 \leq h/s_1 \leq 1.8 \\ &= 0.35 + 0.183 \cdot h/s \text{ if } 1.8 \leq h/s_1 \leq 3 \\ &= 0.9 \text{ for } h/s_1 > 3 \end{aligned}$$

h is the height of the ice area, found from section 7.2.1 in [DNVGL (2016)]
t_c is an increment for abrasion and corrosion, given in mm. Usually taken as 2.

The contact pressure used in Equation (3.2) and (3.3) are based on compressive tests of ice. These tests found the crushing pressure of unconfined, low strain rate specimens to be between 1.5 to 3.0 MPa for first-year and multi-year ice. To account for the fact that the ice might be confined in the transverse direction, this

strength should be multiplied with a factor of 2. For higher strain rates, the crushing pressure increases, and 5.6 MPa has been chosen as a standard value for the rules [DNVGL (2005)].
With regards to material selection, the Cold Climate rules only sets requirements to parts exposed to cold weather. These members are to have steel grades not lower than given in Figure 3.1. For materials not exposed to weather, the requirements are given by DNVGL-RU-SHIP-Pt.3 Ch.3, which covers structural design principles for the hull.

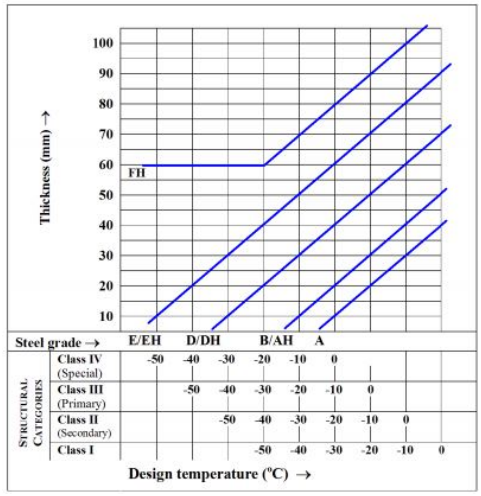

Figure 3.1: The required steel grade depending on thickness and temperature, courtesy to DNV GL(2016).

As seen from Figure 3.1 the material requirements varies depending on the class of the member in question. Excerpts of the tables describing the different structural classes is given in Appendix A. Figure 3.1 shows that the material requirements becomes stricter as the temperature and thickness of the member increases. For side plating with thickness of 20 mm the required material grade is A if the design temperature is -10°C and higher, but if the design temperature is $\leq$ 20°C a grade B or AH material is required. In an Arctic environment with an even lower design temperature, a class D/DH or E/EH material would be required for the same member.

3.2 DNV GL Standard - Design of Offshore Steel Structures

3.2.1 Plate Thickness Requirements

The DNV GL Design of Offshore Steel Structures (2015) rules are based on linear theory, calculating the minimum thickness of plates based on yield stress. However,

as the Cold Climate rules calculates plate thickness with respect to ice load, the Design of Offshore Steel Structures and the Cold Climate rules will differ in the required thickness.

DNVGL-OS-C101 requires the plate to be thicker than the thickness defined in Equation (3.4) if the plate is not exposed to lateral loads, Equation (3.5) if exposed to lateral loads [DNVGL (2015)].

$$t = \frac{14.3t_0}{\sqrt{f_{yd}}}[mm] \tag{3.4}$$

$$t = \frac{15.8K_a s\sqrt{p_d}}{\sqrt{\sigma_{pd1}k_{pp}}}[mm] \tag{3.5}$$

where:

f_{yd} = design yield strength
t_0 = 7 mm for primary structural elements, 5 mm for secondary structural elements
K_a = correction factor for aspect ratio of plate field
s = stiffener spacing
p_d = design pressure
σ_{pd1} = design bending stress
k_{pp} = fixation parameter for plate

3.2.2 Material requirements

The material requirements of the DNV GL Design of Offshore Steel Structures (2015) are based on the nominal thickness. Different steel grades are required depending on the thickness and the service temperature. Table 3.1 illustrates an excerpt of the maximum thickness table given in the rules [DNVGL (2015)]. As seen from Table 3.1, the maximum allowed thickness decreases with temperature. The material requirements also varies depending on the location and function of the component. For a certain component with a required thickness, the material selection will have to be adjusted to reflect the service temperature.

3.3 Floating Offshore Structures

The ISO 19904-1, Floating Offshore Structures (2006) code has no specific requirements to the plate thickness. It does however, state that linear and non-linear analysis might be used for ULS-checks, while non-linear analysis is required for ALS. While no specific requirements is made for the thickness of the plate, requirements are made for the model used for analysis. Among other modelling requirements, a large-volume component, such as the ship side modelled in this report, shall be modelled with three-dimensional shell models.

Table 3.1: Excerpt of the thickness limitations [mm] of structural steels for different structural categories and service temperatures [° C] table, from [DNVGL (2015)].

Structural Category	Grade	≤ 10	0	-10	-20	-25	-30
Secondary	A	35	30	25	20	15	10
	B/BW	70	60	50	40	30	20
	D/DW	150	150	100	80	70	60
Primary	A	30	20	10	N.A.	N.A.	N.A
	B/BW	40	30	25	20	15	10
	D/DW	70	60	60	40	35	30

With respect to material selection, ISO 19904-1 does require that the consequence of failure, the presence of stress concentrations and minimum water and/or air temperature is taken into account. It does not give any specific requirements to the material used, but the code refers to requirements given by RCS. Due to the Floating Offshore Structures codes (2006) general nature with respect to plate thickness and material selection, it will not be discussed further.

3.4 UR S6 Material Requirements

In IACS UR S6 (2016) the different structural elements are divided into different categories, depending on where they are and which function the element has. An overview of the different categories and their mechanical properties, are presented in Appendix B, Table B.2.
The materials are divided into three classes, class I, II and III, which depends on where on the ship the material is to be used. A table of classes and structural member category can be found in Appendix B, Table B.1
In Table 3.2, the steel grades are defined as in Appendix B. Table 3.2 is for material class I, tables for class II and III can be seen in Tables B.3 and B.4. As displayed in the tables, the requirement for the steel gets gradually stricter as the temperatures decrease. Implying that the DAT will have great impact on the choice of material for the ship, and might have great influence on the cost of materials. However, for materials below the lowest ballast line, the temperatures are not taken into account for the choice of steel. As the water will not be colder than about -2°C, the submerged steel will not reach very low temperatures.

3.5 Direct Ice Impact

According to ISO 19904 (2006), encounters with sea ice and/or icebergs shall be considered where there is a risk of such an impact. ISO 19904 states that the mechanical properties, the geometry and the failure modes as a function of temperature and other relevant parameters shall be considered. Only a simplified analysis will be carried out in this report, leading to such properties being neglected and the

Table 3.2: IACS material grade requirements for material class I.

Plate Thickness, in mm	**-20/-25 °C**		**-26/-35 °C**		**-36/-45 °C**		**-46/-55 °C**	
	MS	**HT**	**MS**	**HT**	**MS**	**HT**	**MS**	**HT**
$t \leq 10$	A	AH	B	AH	D	DH	D	DH
$10 < t \leq 15$	B	AH	D	DH	D	DH	D	DH
$15 < t \leq 20$	B	AH	D	DH	D	DH	E	EH
$20 < t \leq 25$	D	DH	D	DH	D	DH	E	EH
$25 < t \leq 30$	D	DH	D	DH	E	EH	E	EH
$30 < t \leq 35$	D	DH	D	DH	E	EH	E	EH
$35 < t \leq 40$	D	DH	E	EH	E	EH	-	FH
$40 < t \leq 50$	E	EH	E	EH	-	FH	-	FH

iceberg will be modelled as a rigid body. This will lead to a conservative analysis, as the ship side will absorb all energy.

3.6 Temperature Effects

Due to the change in material properties with temperature, the design ambient temperature (DAT) is of great importance for the choice of material. The standards defines different design temperatures. DNV GL defines the DAT as the lowest mean daily average temperature (LMDAT). On the other hand ISO 19904-1 defines the DAT as the lowest anticipated service temperature (LAST). LAST is defined as the lowest one-hour average temperature associated with an annual probability of exceedance of 10^{-2}[ISO (2006)].

To find LMDAT of an area, historic temperature data is required. IACS (2016) requires a 10 year period of statistical data for the area of operation. To calculate LMDAT, the daily average of each day needs to be computed. Using the daily average temperatures, the mean temperature for each day of the year is calculated. The lowest of these mean temperatures is used as DAT. This gives LMDAT as given in Equation (3.6), where $\bar{T}_i$ is the daily average temperature for day i of the year and n is the number of years worth of data.

$$\text{LMDAT} = min\left(\frac{\sum_1^n \bar{T}_i}{n}\right) \tag{3.6}$$

To find LAST, a probability function needs to be fitted to the temperature data. Using this probability function, a long term distribution, F, can be found. By solving Equation (3.7), with 8760 as the number of one-hour events in a year, the LAST can be found.

$$1 - F = \frac{10^{-2}}{8760} \tag{3.7}$$

Due to the temperature fluctuations being greater for short periods of time, it is

reasonable to assume that the LAST will be lower than LMDAT for a specified area. This will lead to a stricter material requirement if the ISO Design of Offshore Structures is used for design, compared to if the design is done on basis of RCS rules. Due to the different definitions of DAT, the design temperature of a vessel might be different for a ship, depending on whether the designer uses ISO or RCS rules.

Chapter 4

Finite Element Modelling

This chapter presents the method used for FEM-modelling. It also presents the assumptions done during modelling of the structures.

4.1 Study of Impacted Plate

To verify the model used, a FEA-study of the drop test done by Kim et al (2016) was repeated. To ensure that the results was comparable, the FEA was conducted as similar as possible to the methods described in the paper by Kim et al (2016). Figure 4.1 shows the complete model of the plate and striker.

The welds were modelled using a separate section to be able to vary the material and the thickness of the section. The thickness in the weld area was increased to 9 mm. The weld section was set to be one element wide, and was added on all welded areas along the stiffener and plate edge. Figure 4.2 shows the stiffener-plate intersection with the increased thickness along the welds. This is in agreement with the methods used by Kim et al (2016). Figure 4.3 and 4.4 shows the areas defined as welds in the Abaqus model marked with red.

In reality material properties in the heat affected zone, HAZ, changes due to the welding. Due to cracks, weld imperfections and residual stresses brittle fracture of the HAZ is a concern. However due to the increased thickness in the welded area, fracture is expected to happen along the edge of the welded area. In the Abaqus model, the material in the welded zone is the same as for as the plate. This is partly done to be comparable to the study done by Kim et al. and partly for simplicity.

To minimize potential sources of error, the FE model was made to be as similar to the actual test as possible. However, due to lack of information on the geometry of the jig and the striker presented in the report, the jig and striker was modelled using measurements done on the images in the report.

In Abaqus the jig was modelled with an inner length of 0.6 meter, i.e. equal to the tested plate, a thickness of 0.02 meter and a height of 0.5 meter. The knees on

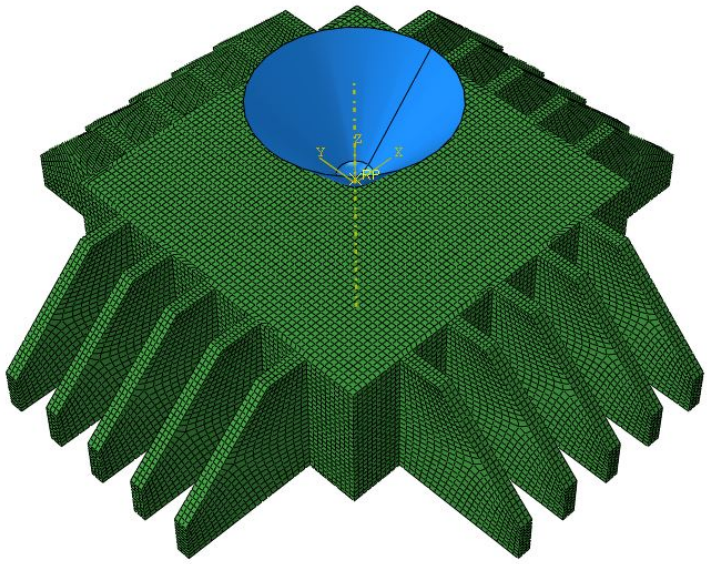

Figure 4.1: Complete model of the plate, jig and striker.

the jig was modelled symmetrical with a long side of 0.5 meters and a short side of 0.15 meters. The entire jig was modelled with the solid C3D8R element.

The impacted plates and stiffeners were modelled with the shell element S4R. The geometry and thickness of the plate and stiffeners was found from the report.

At the time of impact, the striker velocity was as given in the report, 7.06 m/s for the RT simulations, and 8.57 m/s for the -60°C simulations. The geometry of the striker was approximated using the images in the report, with the dimensions as shown in Figure 4.5.

The material model was based on the power hardening law, as given in Equation (4.1). In addition, strain rate effects was modelled using the Cowper-Symons equation, Equation (4.2), as done by Kim et al. (2016). The material parameters used are given in Table 4.1. As Abaqus does not have any of these material models implemented, the material parameters were given as tabulated data from Matlab. Failure was modelled using the failure strain criteria. Kim et al (2016) presents Equation (4.3), where ϵ_{fcr} is the critical fracture strain, ϵ_f is the fracture strain obtained from the experiments, t is the plate thickness and S is the element size, for finding the critical failure strain for the model from the material tests carried out. By using this equation, the failure strains are found to be 1.46 for 20°C and 1.36 for -60°C. This does not correspond with the plot presented in the same paper, where the failure strains for -60°is found to be approximately 0.075 and the failure strain for 20°is found to be 2.26. Due to this, both failure strains were used. In Section 5.1 these two different failure criteria will be called ”fracture criteria from equation” and ”fracture criteria from figure”.

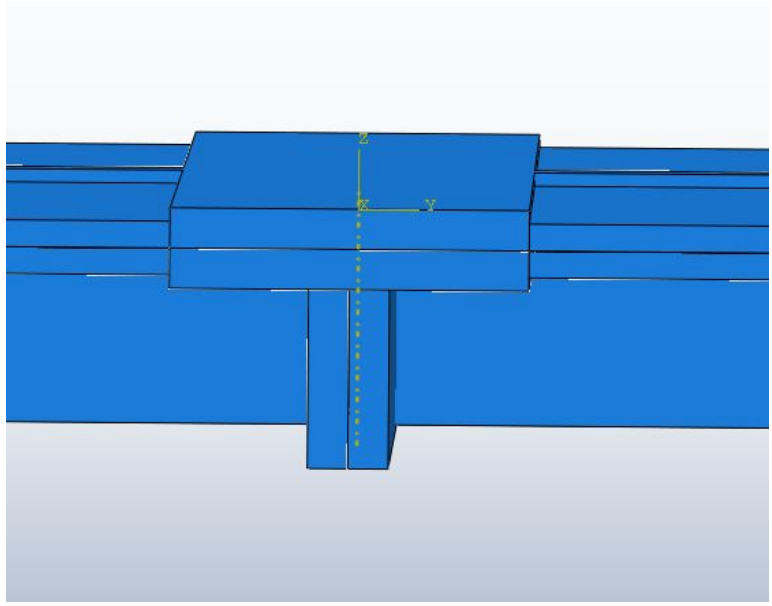

Figure 4.2: The plate-stiffener intersection with the increased thickness visible.

$$\sigma = K \cdot e^n \tag{4.1}$$

$$\frac{\sigma_{yd}}{\sigma_y} = 1 + (\frac{\dot{\epsilon}}{C})^{\frac{1}{q}} \tag{4.2}$$

$$\frac{\epsilon_{fcr}}{\epsilon_f} = 4.1 + \frac{t}{S}^{0.58} \tag{4.3}$$

Table 4.1: Material parameters.

Parameter	Temperature	Value
n	RT	0.214
	-60°C	0.232
K	RT	936.2
	-60°C	1103.8
C	-	3200
q	-	5

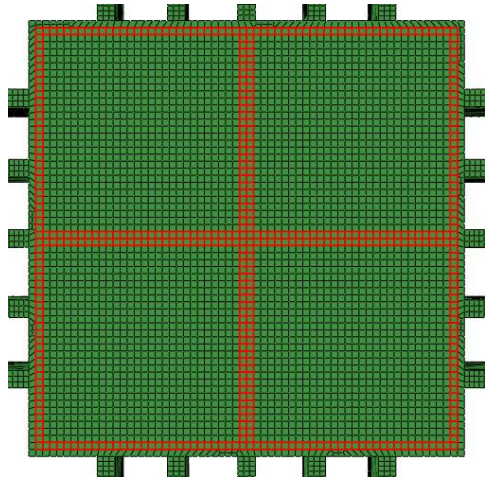

Figure 4.3: The welded areas on the plate surface.

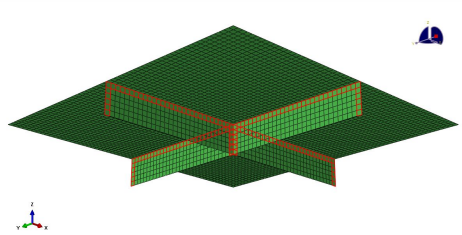

Figure 4.4: The welded areas of the stiffeners.

4.2 Testing of Woongshik Nam Material Model

For testing of the material model developed by Woongshik Nam, a VUMAT supplied by Woongshik Nam was used. The FEM model used was the same as described in Section 4.1. The VUMAT was applied to the plate and stiffeners, while the jig used the same material as in the previous analysis. The same two analyses as described in Section 4.1 were repeated using the material code supplied by Woongshik Nam. To account for the effect of temperature on yield stress, the yield stress was taken from Park et als (2012) study on material parameters, as described in Section 4.3.2.

For the remainder of the thesis, this material will be called Nam material.

4.3 Ship Side Impact

For large scale testing, a Patran model of a DNV GL ICE-A classed cruiseferry was supplied by Suyu Wang, which was created as part of his master thesis [Wang

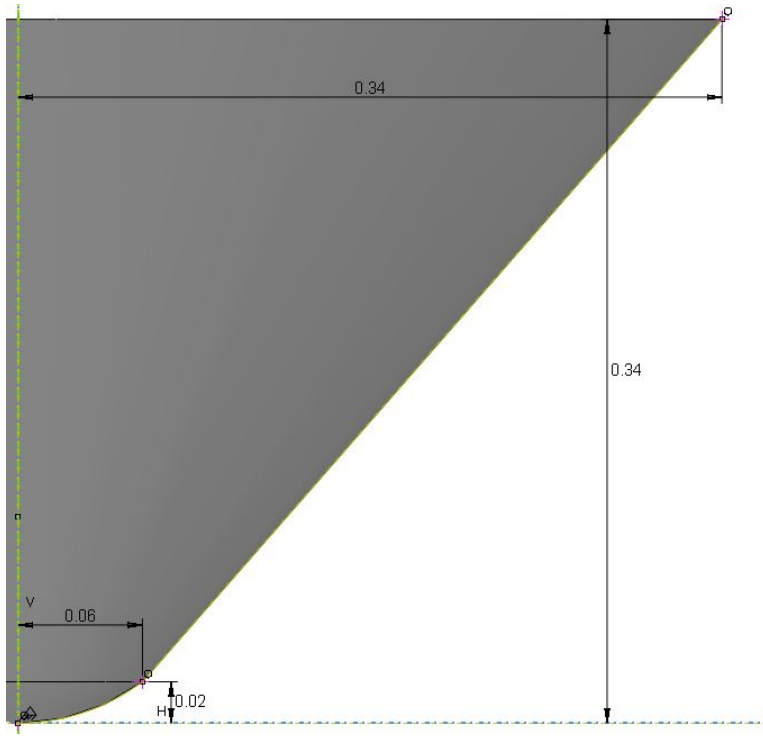

Figure 4.5: The dimensions of the striker, given in meters.

(2017)]. This model is of frame 200 to 215 of the vessel, which is the fore part of the vessel. The whole model is modelled using a varying element size. For more information on the modelling of the ship, see Wangs master thesis. The vessel has a LOA of 223.9 m and a LPP of 202.66 m. The Patran model supplied did not include the thickness of plates, which was found using section drawings of the hull. The whole model is built using a combination of S4R and S3R elements, where the quadratic S4R element is preferred, and is used on all elements which has a quadratic shape. Some details on the ship had to be modelled using the triangular S3R element to avoid excessive distortion of the elements. All edges of the model has been locked for all rotations and translations. In Figure 4.6 the complete ship side with the ice body is displayed.

4.3.1 Ice Body

The ice body was modelled as circular a disk with a diameter of 10 meters and a thickness of 1.2 meter. It was modelled using a analytically rigid shell structure. The mass of the ice body was set to 1000 tonnes and an initial velocity of 6 m/s. It was locked in all translations, with exception of the direction of impact. The impact was set to be at the waterline in the centre of the model. From the lower

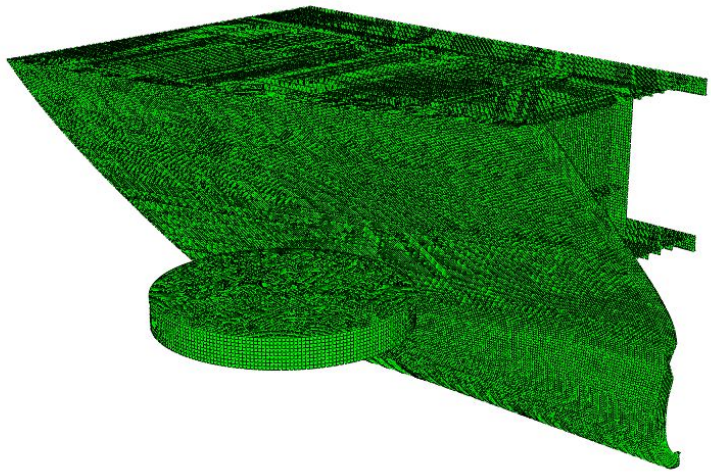

Figure 4.6: The complete ship side model and the ice body.

forward corner of the model, the impact was located at 10.454 meters along the length of the hull and 6.4 meter above the bottom line.

As no ice model was found for Abaqus, as stated in Section 2.5, the ice body was modelled as rigid.

4.3.2 Steel Material Parameters

A study of the effects of low temperatures on ASTM A131 steel was carried out by Park et al. (2012). In their study, tension and impact tests were carried out on different shipbuilding steels, among them AH36 and DH36, the steel types used for the drop test described in Section 4.1 and for the ship side. These materials were experimentally tested at temperatures ranging from -160°C to room temperature. From the results presented in their report, the open source Matlab program Grabit by Doke (2016) was used to extract points corresponding to the relevant materials, and Matlab was used to fit functions to these points. The figures giving yield strength and fracture strain are shown in Figure 4.7 and 4.8, which gave the functions shown in Equation (4.4) and (4.5), where t is the temperature in °C.

$$\begin{aligned}\sigma_{y,AH36} = &-6.59\exp{-10}\cdot t^4 - 2.16\exp{-06}\cdot t^3 \\ &+8.46\exp{-3}\cdot t^2 - 0.021\cdot t + 398.69\end{aligned} \tag{4.4}$$

$$\begin{aligned}\epsilon_{f,AH36} = &\ 1.25\exp{-12}\cdot t^4 - 1.12\exp{-10}\cdot t^3 \\ &-9.49\exp{-07}\cdot t^2 - 1.91\exp{-4}\cdot t + 0.37\end{aligned} \tag{4.5}$$

The material code supplied by Woongshik Nam included failure criteria for

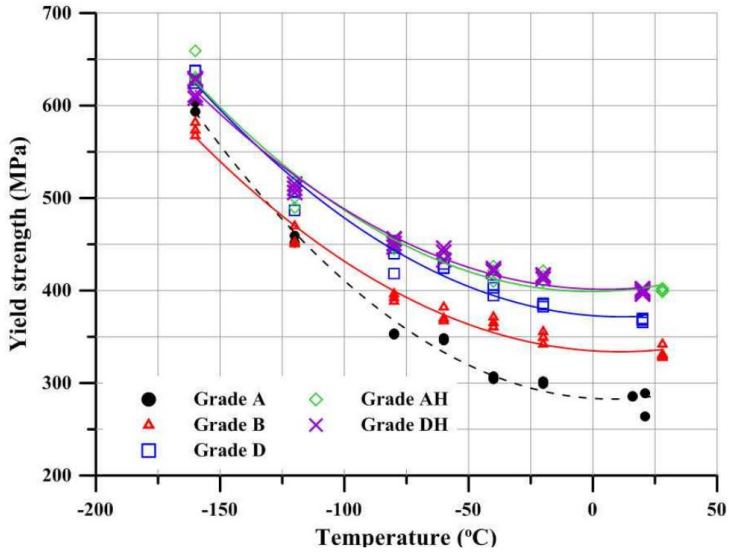

Figure 4.7: Yield stress as a function of temperature, courtesy to Park et al. (2012).

-60°C, -100°C and -140°C. To investigate for other temperatures, an exponential interpolation has been carried out. It should be noted that all other temperatures than -60°C, -100°C and -140°C will not necessarily have correct critical strain energy values. As the critical strain energy has not been validated for other temperatures than these three, the failure mode might be wrong. It should however be sufficient to show the phenomenon of brittle fracture and DBFT, even though the transition temperature might be wrong. At -40°C and at room temperature, the failure criteria for -60°C has been used. As the interpolated criteria was made by interpolating between the temperatures -60°C and -140°C, it is less likely to reflect the real values of critical SED outside this range. At -40°C and at room temperature, only the yield stress and Young's modulus for the material has been changed.

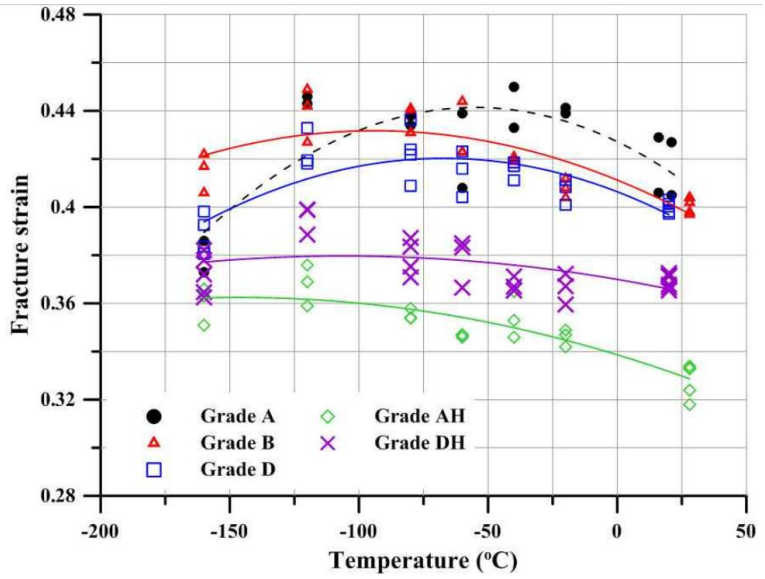

Figure 4.8: Fracture strain as a function of temperature, courtesy to Park et al. (2012).

Chapter 5

Results

This chapter presents the results from the two sets of analyses done and discussion of the results. It will present the results from the Kim drop test first, followed by the results from the ship side collision. Note that the deformation has not been scaled on any of the figures presented in this chapter.

5.1 Impacted Plate Result

This section presents the results from the Kim drop test analysis.

5.1.1 Stiffened Plate

Figure 5.1 shows the displacement pattern and the failure of the plate when using the normal material and the failure criteria from the figure presented in Kim et al (2016). In Figure 5.2 the impacted plate with the normal material and the failure criteria described in Equation (4.3) is shown. As seen, there is no failure in Figure 5.2.

Figure 5.3 shows the centre displacement of the plate using the normal material. The displacement is identical for the first part of the plot. It is also visible that the failure causes a larger displacement. The fracture happens along the edge of the welded area, as expected due to the increased thickness of the welded zone. However, the fracture is smaller and more local than the damage shown by Kim et als (2016) report.

At room temperature there is no fracture with either of the fracture criteria. As only the fracture strain is modified on the two different materials, the displacement and stress pattern is identical at room temperature. Figures showing the displacement patterns of both materials and temperatures are presented in Appendix C.

There is no failure in the plate using the Nam material at -60°C. This is probably due to the material model being slightly non-conservative, which corresponds to the findings presented in Nams (2017) paper. Due to this, the Nam material will

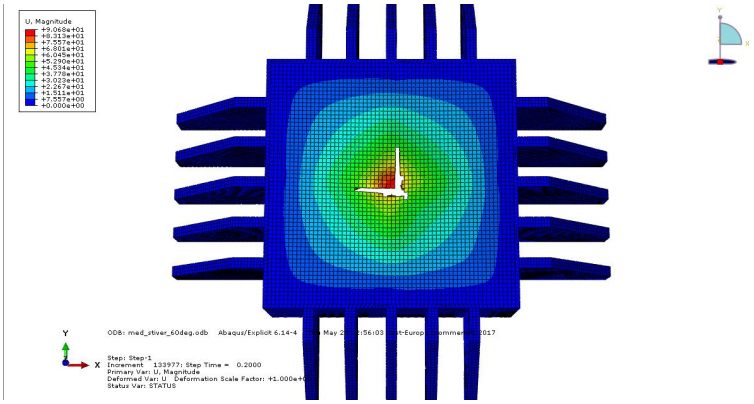

Figure 5.1: The displacement pattern at -60°C using Kim failure criteria from equation.

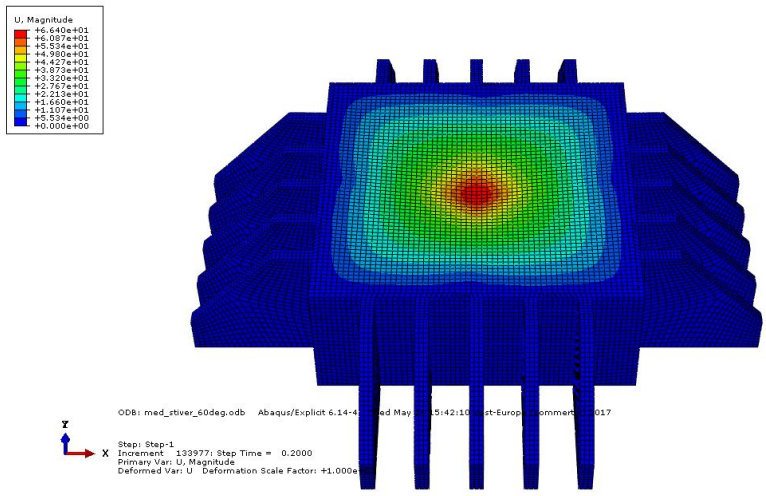

Figure 5.2: The displacement pattern at -60°C using Kim failure criteria from figure.

be compared to the normal material using the failure criteria from Equation (4.3) in Section 5.1.3, as the lack of fracture makes the two materials more comparable

At room temperature, the displacement patterns are reasonably similar. Neither the normal or the Nam material experience any failure. It is noted that the displacement is larger at lower temperatures, which is an effect of the higher impact velocity at -60°C.

5.1.2 Unstiffened Plate

Figure 5.4 and 5.5 shows the displacement pattern using the two failure criteria described in Section 4.1. The two figures are with the fracture criteria from the

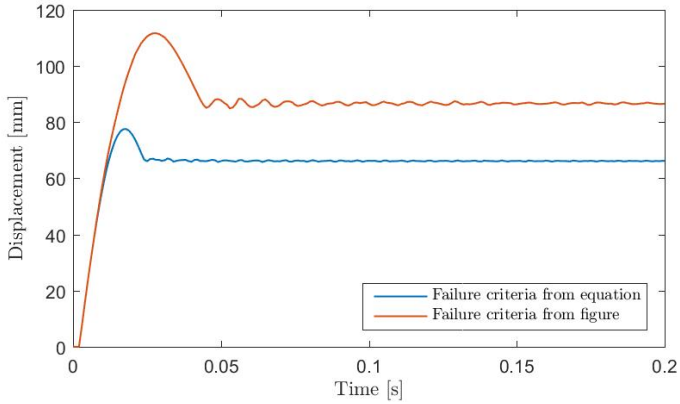

Figure 5.3: The centre displacement for the stiffened plate at -60 °C for the two different failure criteria.

figure and equation, respectively. As seen in Figure 5.4, there is a failure in the plate using the failure criteria from the figure. The same failure is not found when using the fracture criteria from the equation. In the experimental result presented by Kim et al (2016) there is no failure for the unstiffened plate at -60°C.

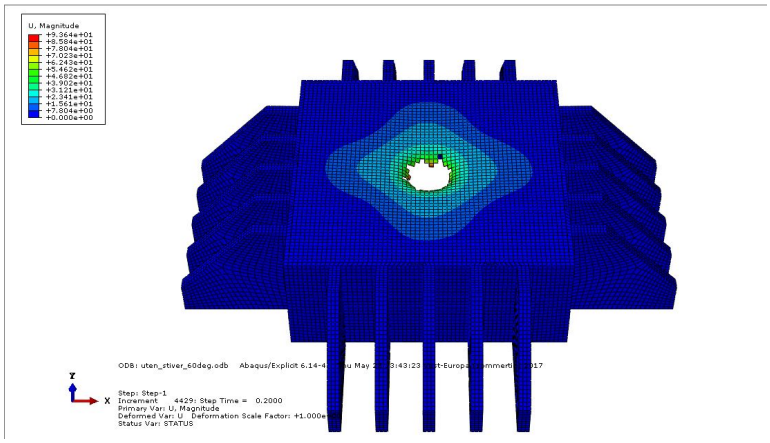

Figure 5.4: The displacement pattern at -60°C using Kim failure criteria from figure.

The displacement pattern for the unstiffened plate using the Nam material is similar to the one found when using the normal material with fracture criteria from the equation and and is displayed in Appendix C.

The Nam material showed a significant spring-back effect, something that was not mirrored in the normal material. This will be further discussed in Section 5.1.4.

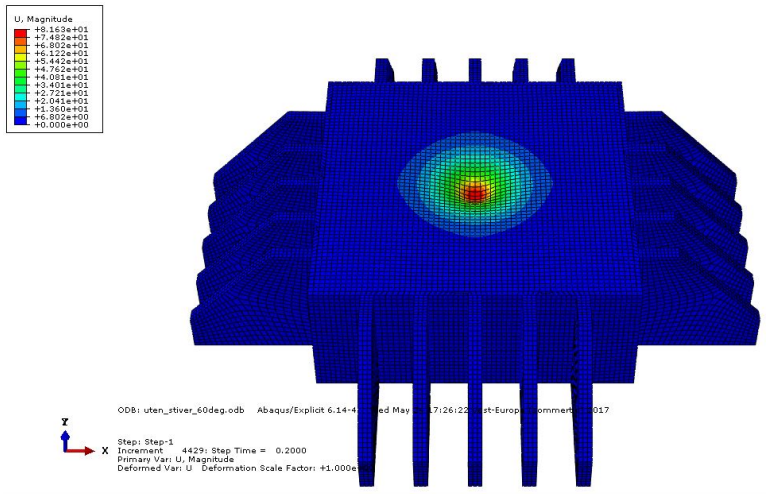

Figure 5.5: The displacement pattern at -60°C using Kim failure criteria from equation. The deformation has not been scaled.

5.1.3 Comparison of Stiffened Plate with Kim and Nam Material

As there was no fracture for the Nam material, it will be compared to the normal material with no fracture, i.e. using the fracture criteria from the equation. Figure 5.6 shows the centre displacement of the plate.

Table 5.1: Centre displacement for stiffened plate.

Temperature and material	max displacement	end displacement
-60°C Nam material	81.91	69.42
-60°C Kim material	77.57	66.21
20°C Nam material	66.70	57.06
20°C Kim material	62.52	51.71
20°C Experimental result	74.9	

From Figure 5.6, it is apparent that the displacement pattern for the two plates are similar. It shows that the Nam material is somewhat softer than the normal material. In addition, some spring-back of the plate is detected. Table 5.1 shows the maximum displacement and the end displacement of the stiffened plate at room temperature and -60°C. Additionally, the measured value from Kim et als (2016) study is included. At -60°C the stiffened plate experienced fracture during the drop test [Kim et al. (2016)], which led to no value being measured for the displacement. However, there was no failure in the Abaqus model. In the case of the normal material, this is due to the fracture strain being to high. The difference in the maximum displacement between the experimental value and FEM results

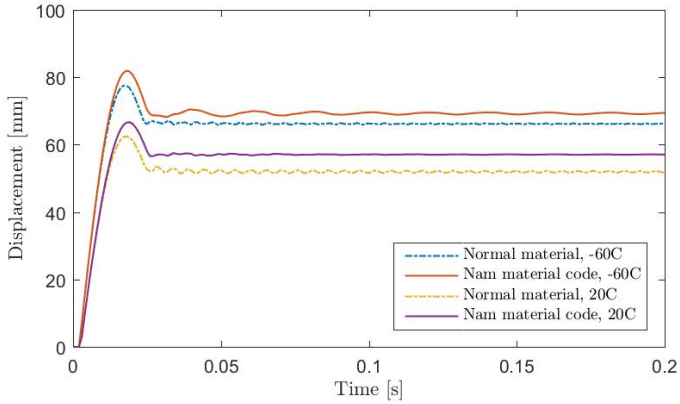

Figure 5.6: The mid-point displacement over time for different temperatures and both materials.

might be due to difference in striker geometry between the two cases. As stated in Section 4.1 no striker geometry was given in the report by Kim et al, and the geometry used in the FEM model is based on measurements done on the figures in the report. This will lead to some inaccuracy in the geometry used in the FEM model, and might be the reason for the discrepancy between the experimental and the modelled displacements.

Figure 5.7 shows the absorbed energy of the plate as a function of time. As seen from the figure, the absorbed energy is close to identical for the two materials.

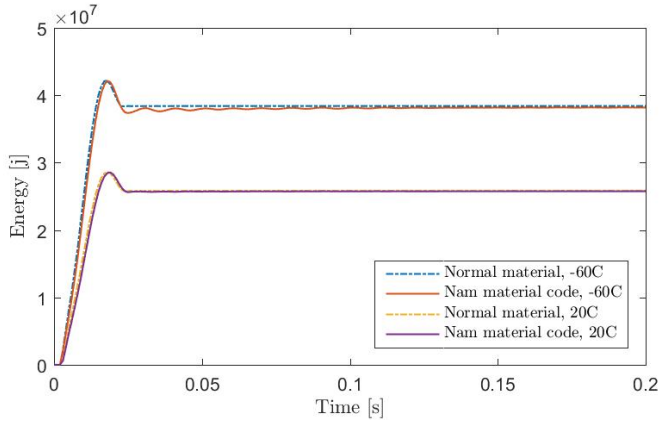

Figure 5.7: The absorbed energy for the stiffened plate for both temperatures and materials.

5.1.4 Comparison of Unstiffened Plate with Kim and Nam Material

Figure 5.8 shows the midpoint displacement over time. When comparing with Figure 5.6 it is apparent that the difference in displacement is larger when the plate is unstiffened. In addition, the shape of the displacement over time is different for the normal material. The normal material show less of a spring-back phenomenon compared to the Nam material.

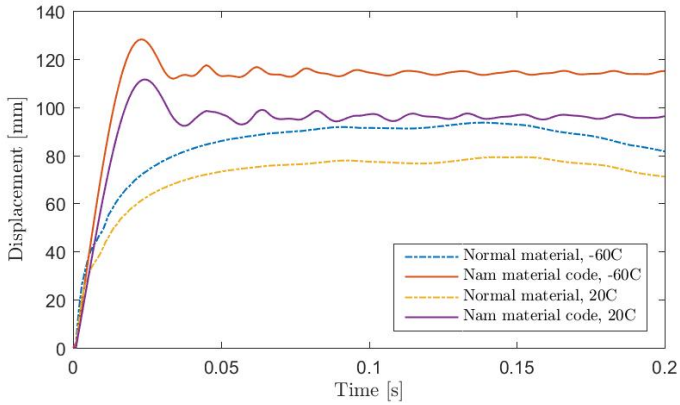

Figure 5.8: The mid-point displacement for the unstiffened plate for both temperatures and materials.

Table 5.2: Centre displacement for unstiffened plate.

Temperature and material	max displacement	end displacement
-60°C Nam material	128.2	115.0
-60°C Kim material	93.56	81.62
20°C Nam material	111.5	96.28
20°C Kim material	79.21	71.08
-60°C Experimental result	104.1	
20°C Experimental result	109.3	

Table 5.2 shows the maximum displacement and the displacement after the end of the simulated time. From the table it is observed that the difference between the two materials is significant. It is also seen that the difference between the experimental results and the modelled result is significant at low temperature. For room temperature, the difference between experimental and Nam material is low. In addition, the highest displacements in the drop test is found at room temperature, while the Abaqus results has the highest displacements at -60 °C.

Figure 5.9 shows the absorbed energy of the unstiffened plate. The figure illustrates that the two materials are not as similar for the unstiffened plate as for the

stiffened plate, due to the difference in displacement pattern. As the two materials do not show the same behaviour in displacement, the absorbed energy over time will differ.

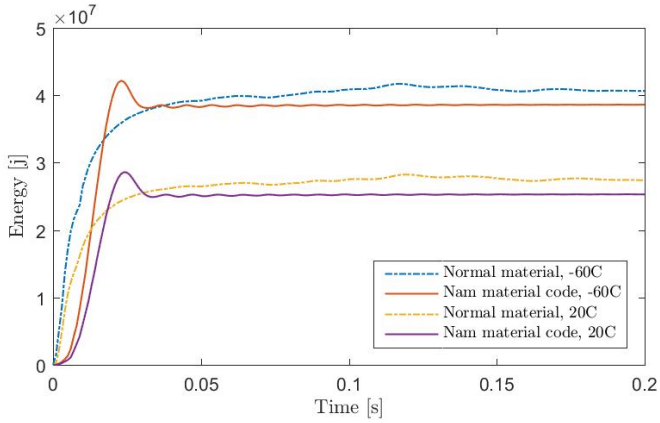

Figure 5.9: The absorbed energy for the unstiffened plate for both temperatures and materials.

5.2 Ship Side Impact

The impact has been carried out at 20°C, -40°C, -60°C, -70°C, -80°C, -90°C and -100°C. Figure 5.10 shows the damaged area of the hull after the impact at -60°C. As the figure displays, there is a small rupture of the plating and the stiffeners are significantly deformed.

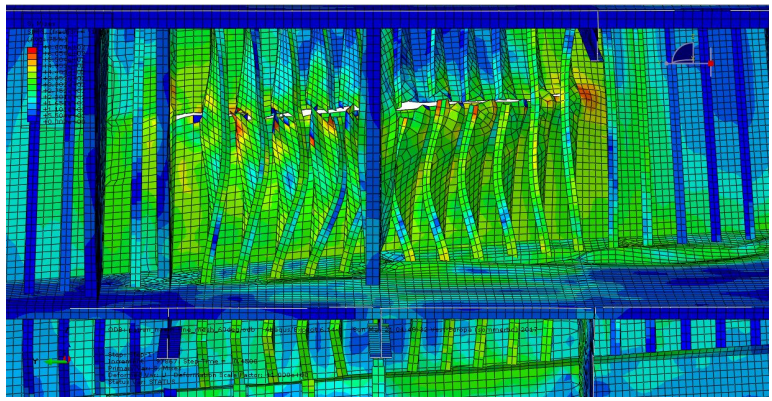

Figure 5.10: The damaged area of the hull after impact at -60°C.

Figure 5.11 shows the damaged area after impact at -90°C. Here the rupture in the plate is larger and has a T-shape. In addition, the deformation of the stiffeners

is larger, some stiffeners have failed and are no longer in contact with the deck plate. The bulkhead in the centre of the picture has buckled and undergoes severe damage.

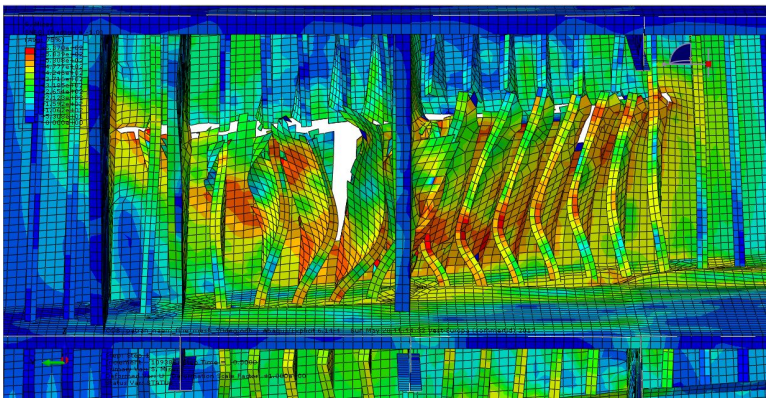

Figure 5.11: The damaged area of the hull after impact at -90°C.

In Figure 5.12 the damage area after impact at -100°C is shown. As seen, a large area of the hull plating is completely destroyed. Several stiffeners have been completely torn of the plate and are currently flying. The bulkhead in the impact zone has been fractured and the bulkhead vertical stiffener has been torn off.

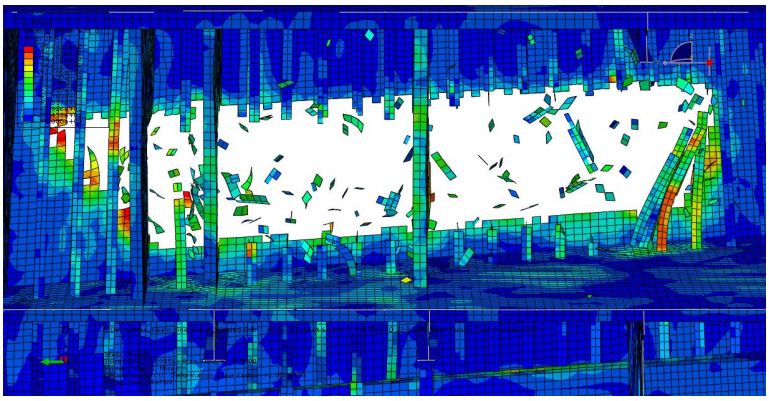

Figure 5.12: The damaged area of the hull after impact at -100°C.

Figure 5.13 displays a side view of the damaged area. In Figure 5.13 a cut has been made through the centre of the displaced area to make the shape of the indentation more visible. As Figure 5.13 displays, the indentation has a sharp corner in the upper part of the impacted zone. This is due to the ice body having sharp edges and being rigid. If an ice model which included crushing of ice had been used, this sharp edge would have been crushed, and the indentation of the hull would have taken a more rounded shape. This sharp edge will lead to higher

damage and increased probability of a rupture of the hull. As the edge hits the ship side, high localized stresses appears at the elements contacting the upper edge of the ice body. These elements are the first elements to fail, and leads to the tear of the hull plates. At room temperature, there is no failure of the stiffeners. All stiffeners are still whole after the collision, while the skin plate ruptures between the stiffeners. At -60 °C several of the stiffeners in the impacted area has failed and has split along the fracture.

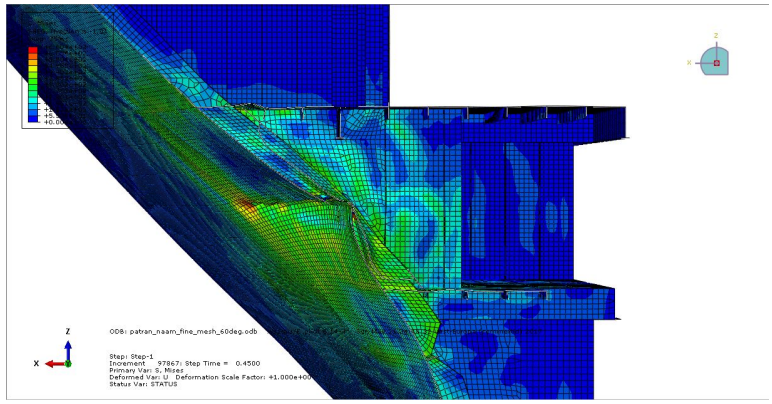

Figure 5.13: A side view of the damaged area after impact at -60°C.

Appendix D shows figures of the damage at the remaining temperatures and the damage from another angle. The damage becomes gradually worse for sinking temperatures. At room temperature, only a small number of elements fracture.

Figure 5.14 shows the logarithm of the mass that has been eroded or is currently not connected to the remainder of the model. Table 5.3 shows tabulated data of how much of the materials mass that has been eroded after 0.5 s. As shown in both Table 5.3 and Figure 5.14 there is a reduction of eroded mass between room temperature and -40°C. As stated in Section 4.3.2, only the yield stress and Young's modulus changed for the impact at -40°C and for room temperature. Leading to the analysis being over-conservative, as the fracture criteria is for -60°C.

However, the increased Young's modulus and yield leads to a decrease in damage. If -40°C is above the DBTT, this result might be representative for the real results. As the Young's modulus and yield stress increases when temperature lowers, the damage resistance of the material will increase with temperature reduction until DBTT is reached. With the data used in this thesis, it might seem like the DBTT for this material is in the -40°C to -60°C range. However, as the data is based on interpolation, this might not be the true DBTT for the material.

In Figure 5.15 the energy absorbed by the plate over time is shown. As presented in the figure, the ship side show some spring-back for high temperatures. When the temperature drops, the absorbed energy peaks later and for -100°C, only about 1/3 of the kinetic energy of the iceberg has been absorbed after 0.5 s. After 0.315 s all energy has been absorbed by the ship side and the iceberg has come to a complete stop at room temperature. In Table 5.4 the absorbed energy and the percentage

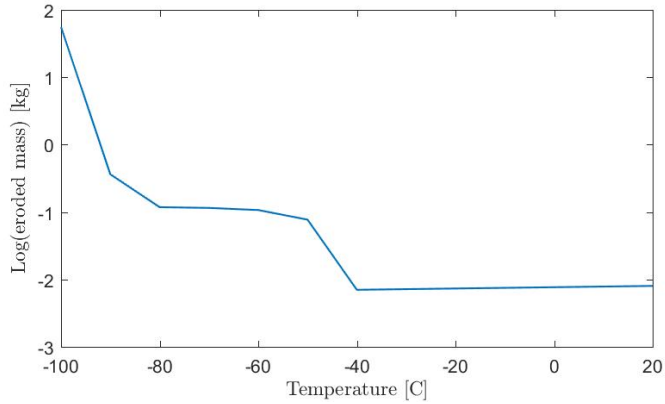

Figure 5.14: The eroded mass at different temperatures. Note that the mass is plotted as the logarithm of the mass on the y-axis.

Table 5.3: The eroded mass and percentage of total model eroded after 0.5 s at different temperatures.

Temperature	Eroded mass [kg]	Percentage of total model mass
Room temperature	8.0	0.0043
-40°C	7.0	0.0038
-50°C	77.0	0.041
-60°C	107.0	0.056
-70°C	115.0	0.062
-80°C	118.0	0.063
-90°C	363.0	0.20
-100°C	55761.0	29.94

of the total energy in the collision has been tabulated. The table shows that there is a gradual drop of absorbed energy as the temperature lowers. In addition, it is seen that the absorbed energy at -70°C is higher than the absorbed energy at -60°C. This is due to the interpolation done to get a critical SED criterion at -70°. If experimental values were used instead of the interpolated values, it would have been expected that the absorbed energy to be lower at -70°C. The table also displays that only 28 % of the energy has been absorbed at -100°C. This means that at -100°C the ice body still has a velocity of 4.32 m/s at the time the ice body has come to a complete stop for the impact at room temperature.

The values used for finding the absorbed energy of the plate is the inverse of the kinetic energy. Ideally, the strain energy would have been used. Due to the material being eroded there is a decline in the overall energy of the system in Abaqus. It might appear as if Abaqus deletes the strain energy of eroded elements. Whether this is a problem with Abaqus or the material model is not known at the current time. However, in the study of the impacted plate using the Nam material,

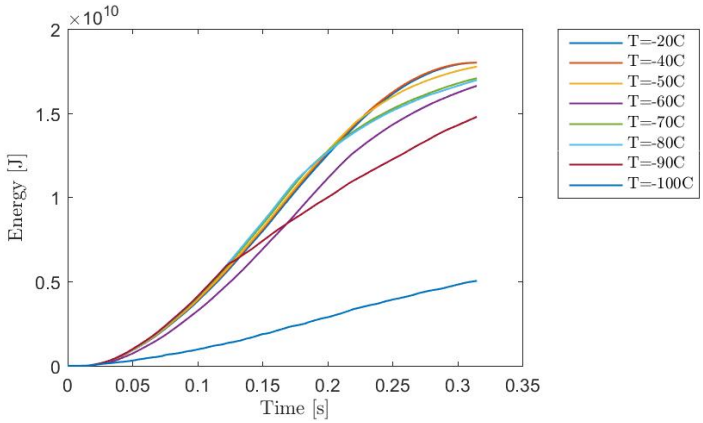

Figure 5.15: The absorbed energy of the ship side.

Table 5.4: The absorbed energy and percentage of total energy absorbed by the ship side after 0.315 s at different temperatures.

Temperature	Absorbed energy [MJ]	Percentage of total energy
Room temperature	18.0	100
-40°C	17.99	99.98
-50°C	17.76	98.66
-60°C	16.62	92.35
-70°C	17.08	94.88
-80°C	16.96	94.24
-90°C	14.78	82.12
-100°C	5.04	27.99

the total energy is conserved, which points towards the erosion of elements being the problem. This will lead to some errors as energy transferred to kinetic energy of stiffeners and loose parts of the plate will not be counted as absorbed energy.

Chapter 6

Discussion

This chapter contains discussion of the results presented in Chapter 5.

The difference in behaviour between the normal material and the Nam material on the unstiffened plate is most probably due to difference in the resistance to bending for the shell. Due to the stiffeners taking some of the bending action from the plate, the difference in bending strength does not affect the stiffened plate. Whether this is due to the tabulated data input for Abaqus being to soft in regards to bending stiffness or the Nam material code being to stiff in bending is unknown. As the model has stiffeners at regular intervals along the whole ship side, the difference in bending stiffness should not be a issue for the ship side model.

The material model supplied by Woongshik Nam provides good results for the temperatures predefined in the code. The interpolation done to cover for the other temperatures might lead to wrong results. As only three temperatures were predefined in the code, an interpolation will be imprecise. The exponential function used was chosen due to the large increase in critical SED at -60°C compared to at -100°C and -140°C. A linear function was considered, but due to the mentioned increase in critical SED the linear function was discarded. In addition, the function was fitted over different temperatures using constant β values. If the β dependant material behaviour changes over the interpolated temperatures, this will not have been captured by the interpolated function.

Some problems have been found with the ship model. There are some hot spots being created due to distorted elements in the mesh. In addition, some stiffener-bulkhead interactions have not been properly assembled in the model. Figure 6.1 shows one of these intersections. As shown in the figure, the elements have not been merged and is overlapping. Two areas have been identified with this problem, one on the fore end of the lowest deck, and one point along the central transverse bulkhead on the top deck. Both these areas were found to late to improve. This does create some artificial stresses in the model, but as all these points are far away from the impact area, it should not influence the results of the impact.

The ship model has been modelled as locked in all rotation and displacements

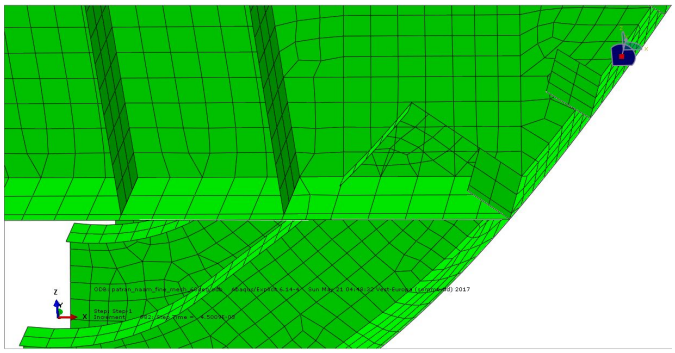

Figure 6.1: A stiffener-bulkhead intersection with element overlap.

along all edges of the model. Due to the difference in the size of the ship and the ice body, this is a reasonable assumption. As the ship is 224 m LOA, compared to the 10 meters of the ice body, the impact should be sufficiently local to not effect the overall motion of the vessel. The ice body is locked for all rotations and all other translations than the impact direction. This is done to simulate a worst case impact, and does not necessarily reflect a real impact. In the case of a floating ice body, the impact might deflect the ice body, and thus reducing the impact of the ship. This could have been modelled by using springs and dampeners to simulate the hydrostatic forces, but this was not done to ensure conservatism in the analysis. In addition, the impact direction and velocity is a worst case scenario. As the ice body has velocity in the transverse direction of the hull, this would imply no velocity for the ship and the iceberg drifting into the ship.

It would have been interesting to investigate how using an ice model instead of the rigid by effects the damage of the hull. If the ice body had not been rigid, the sharp edge would have been crushed, and the ice body would have gotten a more rounded edge. This would have resulted in lower probability of a rupture of the skin plates. The deformation of the ice body would have absorbed some of the energy from the collision. As the energy would have been shared between the ice body and the ship side, the deformation of the ship side would have been reduced. But as no ice model is available for Abaqus it has not been done.

It should be noted that the lowest temperatures tested is below what would be expected in an Arctic environment. Temperatures of -50°C is possible in the Arctic, but the steel will likely be slightly warmer due to the water temperature. As sea water freezes at -2°C, the submerged part of the hull will not be exposed to very low temperatures. The steel in the skin plates will have a gradual decrease in temperature with height over sea level. However, it is possible for the steel to reach very low temperatures in the event of a LNG spill, as natural gas condenses at a temperature of -160°C. The results shows the expected trend; a significant increase in damage when the material temperature decreases. The increase in damage is at a lower temperature compared to the expectations before starting the analysis.

Chapter 7

Conclusion and further work

7.1 Conclusion

A clear correlation between damage and low temperatures has been found. The increase in damage is apparent at -90°C and -100°C compared to the damage at -60°C. At most of the temperatures tested in this thesis the hull ruptures, a possible threat to the safety of the vessel. For the two lowest temperatures, -90°C and -100°C, the damage is large enough to be critical to the safety of the vessel. The damage to the hull at these two temperatures is large enough to lead to rapid flooding of the fore part of the vessel.

The energy dissipation have been found to depend on the temperature of the steel. As the temperature sinks, the time before the collision energy has dissipated increases. This is due to the materials' ability to absorb energy without failing being reduced. At -100°C the damage to the hull is extensive, and only 38% of the total energy is absorbed at the end of the simulation.

A small increase in resistance is found between 20°C and -40°C. This might be due to the way the material was defined for these temperatures, but the result is likely to reflect the real behaviour of the material. For steel, the material strength should increase as the temperature closes to the DBTT due to material hardening. However, as soon as the DBTT is reached, the brittleness of the material will lead to a reduction in strength. This phenomenon seems to be slightly reflected in the result at -40°C, but further studies is needed to draw a conclusion regarding this.

The material parameters for -60°C and -100°C in the used material code was predefined in the code and should give accurate results. For the temperatures between these two, interpolation has been carried out to find a critical SED. This leads to the results found for these intermediate temperatures being uncertain, but it should be accurate enough to show the trends.

7.2 Further work

As mentioned in Chapter 6, it would have been interesting to investigate how using an ice material model affects the damages after impact. Using an ice model would lead to the collision energy being distributed between the hull and the ice body. In addition, the sharp edge of the ice body would have been crushed and the edge would have been rounded. This would lead to an increase of impacted area and probably reduce the risk of rupture of the hull. The increase of area would most likely have led to larger deformations, as the energy would have been distributed over a larger area. How the temperature of the ice and metal effects this energy distribution is still unknown. Ice becomes more brittle as the temperature declines, which should lead to less damage for the hull. However, with the increase in brittleness, the hardness of the ice increases. Whether this increase in hardness will lead to larger damage or the brittleness of the ice reduces the damage will have to be investigated in the future.

The DBTT zone should be identified more closely and the crashworthiness should be investigated in this zone. It is expected that the material will be stronger for temperatures close to the DBTT, but this will have to be investigated. As stated earlier, it is expected that the impact strength of the material will rise due to the increase in yield strength and Young's modulus.

As only the critical SED was defined for certain temperatures, finding the critical SED for the intermediate temperatures will be important to improve the result presented in this thesis. The interpolation done to cover for the intermediate temperatures gives uncertainty to the results. To properly conclude whether a small decrease in temperature increases the crashworthiness, simulations will have to be done with correct critical SED values.

Bibliography

Abaqus (2009). Abaqus 6.13 theory guide. `http://129.97.46.200:2080/v6.13/books/stm/default.htm`. Accessed: 2016-11-07.

Alsos, H., Hopperstad, O., and Amdahl, J. (2009). On the resistance to penetration of stiffened plates, part II:Numerical analysis. *International Journal of Impact Engineering*.

Amdahl, J. (2015). *Buckling and Ultimate Strength of Marine Structures*. NTNU.

Bhadeshia, H. and Honeycombe, R. (2006). *Steels, microstructure and properties*. Elsevier Ltd, 3 edition.

Callister, W. D. and Rethwisch, D. G. (2011). *Materials Science and Engineering*. John Wiley and Sons Pte Ltd, 8 edition.

DNVGL (2005). Rules background, part 5 , chapter 1, section 3 - ice strengthening in the northern baltic. Technical report, DNV-GL.

DNVGL (2010). Shipping across the arctic ocean, a feasible option in 2030-2050 as a result of global warming?

DNVGL (2015). Dnvgl-os-c101 - design of offshore steel structures, general - lrfd method. Technical report, DNV GL.

DNVGL (2016). Dnvgl-ru-ship pt6. ch6 - rules for classification, ships, part 6, additional class notations, chapter 6 cold climate. Technical report, DNV GL.

Doke, J. (2016). Grabit. `https://se.mathworks.com/matlabcentral/fileexchange/7173-grabit`. Accessed: 2016-05-20.

Ehlers, S. and Ostby, E. (2012). Increased crashworthiness due to arctic conditions - the influence of sub-zero temperature. *Marine Structures*, 28(1):86 – 100.

Ferrari, N. (2014). Model for ice material properties in iceberg-ship collision analyses by finite elements. Master's thesis, University of Genoa, Polytechnic School.

IACS (2016). Ur s - requirements concerning strength of ships. Technical report, International Association of Classification Societies.

ISO (2006). 19904-1: 2006 "floating offshore structures, part 1: Monohulls, semi-submergibles and spars". Technical report, International Standard Organization.

Kim, K. J., Lee, J. H., Park, D. K., Jung, B. G. J., Han, X., and Paik, J. K. (2016). An experimental and numerical study on nonlinear impact responses of a steel-plated structures in an Arctic environment. *International Journal of Impact Engineering*.

Liu, Z., Amdahl, J., and Løset, S. (2011). Plasticity based material modelling of ice and its application to ship-iceberg impacts. *Cold Regions Science and Technology*.

Moore, P., Jordaan, I., and Taylor, R. (2011). Explicit finite element analysis of compressive ice failure using damage mechanics. *Proceedings of the 22nd International Conference on Port and Ocean Engineering under Arctic Conditions*.

Nam, W. (2017). Numerical study on ductile-brittle fracture transition (dbft) for large shell element. Work in progress, currently not published.

Nam, W. and Amdahl, J. (2016). Influence of brittle fracture on the crashworthiness of ship and offshore structures in Arctic conditions.

Park, D. K., Kim, D. K., Kim, B. J., Seo, J. K., and Paik, J. K. (2012). Effects of low temperature on astm a131: An experimental and numerical study. *Proceedings of the ASME 2012 31st International Conference on Ocean, Offshore and Arctic Engineering*.

Storheim, M. (2015). *Structural response in ship-platform and ship-ice collisions*. PhD thesis, Norwegian University of Science and Technology.

Tippmann, J. D. (2011). Development of a strain rate sensitive ice model for hail ice impact simulation. Master's thesis, University of California, San Diego.

Wang, S. (2017). Analysis of accidental iceberg impacts with large passenger vessels. Master's thesis, Norwegian University of Science and Technology.

Appendix A

Tables from DNVGL rules

A.1 DNVGL Cold Climate structural categories

The following tables are excerpts from the tables of structural categories presented in Pt. 6, Ch. 6 Sec. 4 of the DNVGL Cold Climate RP

- Class IV
  - Strakes in the strength deck and shell plating amidships indented as crack arrestors.
  - Highly stressed elements in way of longitudinal strength member discontinuities.
- Class III
  - Plating chiefly contributing to the longitudinal strength.
  - Fore ship substructure for vessels with class notation **Icebreaker**.
  - Appendages of importance for the main functions of the ship, e.g. stern frames, rudder horns, rudder, propeller nozzles and shaft bracket.
  - Foundations and main supporting structures for heavy machinery and equipment
- Class II
  - Structures contributing to longitudinal and/or transverse hull girder strength in general.
  - Structures for subdivisions.
  - Structures for cargo, bunkers and ballast containment.
  - Internal longitudinal members (stiffeners, girders) on plating exposed to external low temperatures where class III and IV is required.

- Class I
  - Local members in general unless upgraded due to special considerations of loading rate, level and type of stress, stress concentrations and load transfer points and/or consequences of failure.
  - Deckhouse or superstructure in general.
  - Cargo hatch covers.

Table A.1: Excerpt of DNVGL Cold Climate material classes of strength members in general table.

Structural member	Within 0.4 L amidships	Elsewhere
Secondary: A1. Longitudinal bulkhead strakes, other than that belonging to the Primary category A2. Deck plating exposed to weather, other than that belonging to the Primary or Special category A3. Side plating A4. Transverse bulkhead plating	II	II
Primary: B1. Bottom plating, including keel plate B2. Strength deck plating, excluding that belonging to the Special category B3. Continuous longitudinal members above strength deck, excluding hatch coamings B4. Uppermost strake in longitudinal bulkhead	III	II
Special: C1. Sheer strake at strength deck C2. Stringer plate in strength deck C3. Deck strake at longitudinal bulkhead, excluding deck plating in way of inner-skin bulkhead of double-hull ships	IV	III

Appendix B

IACS Tables

The material classes and grades for ships intended to operate at temperatures below and including $-20°C$ are defined in Table B.1.

Table B.1: UR S6 Material classes and grades for structures exposed at low temperatures.

	Material Class	
Structural member category	Within 0.4L amidships	Outside 0.4L amidships
Secondary: Deck plating exposed to weather, in general Side plating above BWL Transverse bulkheads above BWL	I	I
Primary: Strength deck plating Continuous longitudinal members above strength deck, excluding longitudinal hatch coamings Longitudinal bulkhead above BWL Top wing tank bulkhead above BWL	II	I
Special: Sheer strake at strength deck Stringer plate in strength deck Deck strake at longitudinal bulkhead Continuous longitudinal hatch coamings	III	II

Table B.2: UR S6 Mechanical properties for various steel grades.

Grade	Yield Strength minimum [N/mm]	Tensile Strength [N/mm	Elongation [%]	Impact test						
				Test Temp °C	Average impact energy minimum [J]					
					t ≤ 50		50 < t ≤		70 < t ≤ 100	
					long	trans	long	trans	long	trans
A	235	400/520	22	+20	-	-	34	24	41	27
B				0	27	20	34	24	41	27
D				-20	27	20	34	24	41	27
E				-40	27	20	34	24	41	27

Table B.3: IACS material grade requirement for material class II.

Plate Thickness, in mm	**-20/-25 °C**		**-26/-35 °C**		**-36/-45 °C**		**-46/-55 °C**	
	MS	**HT**	**MS**	**HT**	**MS**	**HT**	**MS**	**HT**
t ≤ 10	B	AH	D	DH	D	DH	E	EH
10 < t ≤ 20	D	DH	D	DH	E	EH	E	EH
20 < t ≤ 30	D	DH	E	EH	E	EH	-	FH
30 < t ≤ 40	E	EH	E	EH	-	FH	-	FH
40 < t ≤ 45	E	EH	-	FH	-	FH	-	EH
45 < t ≤ 50	E	EH	-	FH	-	FH	-	EH

Table B.4: IACS material grade requirement for material class III.

Plate Thickness, in mm	**-20/-25 °C**		**-26/-35 °C**		**-36/-45 °C**		**-46/-55 °C**	
	MS	**HT**	**MS**	**HT**	**MS**	**HT**	**MS**	**HT**
t ≤ 10	D	DH	D	DH	E	EH	E	EH
10 < t ≤ 20	D	DH	E	EH	E	EH	-	EH
20 < t ≤ 25	E	EH	E	EH	E	FH	-	FH
25 < t ≤ 30	E	EH	E	EH	-	FH	-	FH
30 < t ≤ 40	E	EH	-	FH	-	FH	-	-
40 < t ≤ 45	E	EH	-	FH	-	FH	-	-
45 < t ≤ 50	-	FH	-	FH	-	-	-	-

Appendix C

Additional figures from the Paik study

This chapter contains additional figures of the results from the FEM analysis of the Paik study. The deformation has not been scaled at any of the following figures.

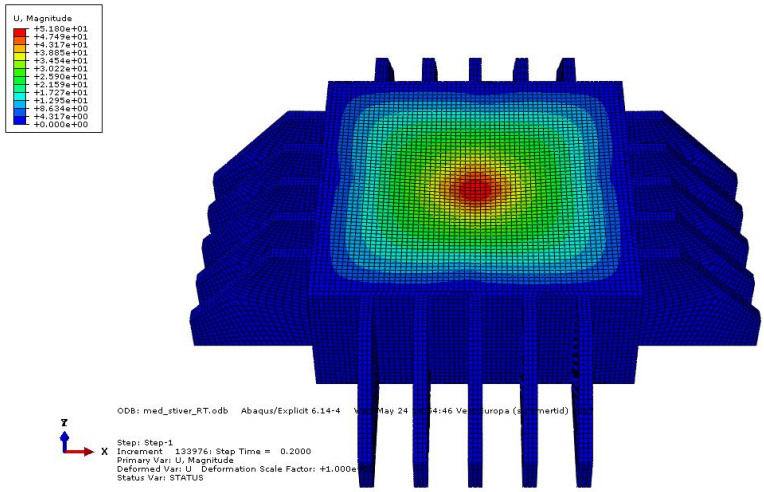

Figure C.1: The displacement pattern for the stiffened plate at room temperature using the normal material.

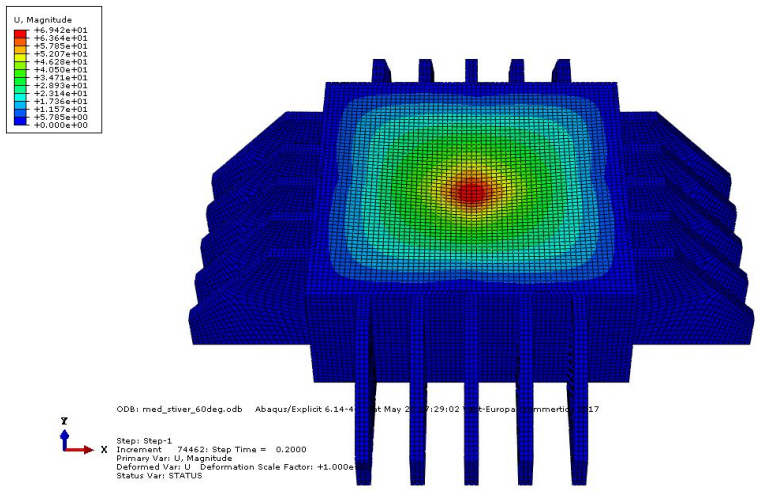

Figure C.2: The displacement pattern for the stiffened plate at -60°C using the Nam material.

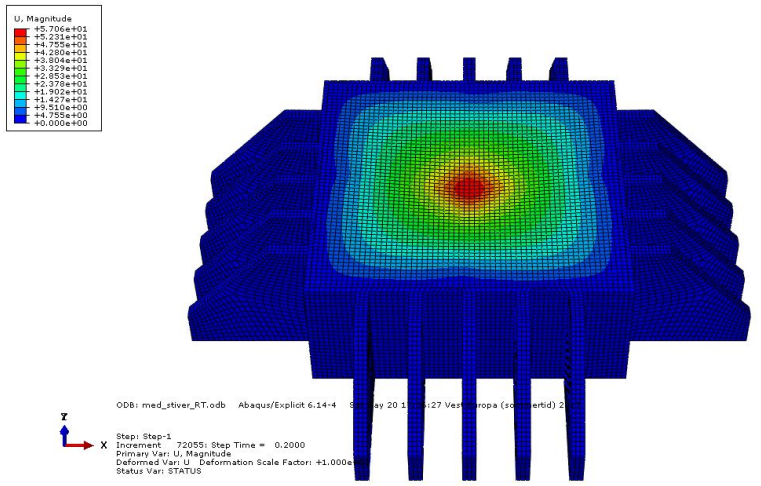

Figure C.3: The displacement pattern for the stiffened plate at room temperature using the Nam material.

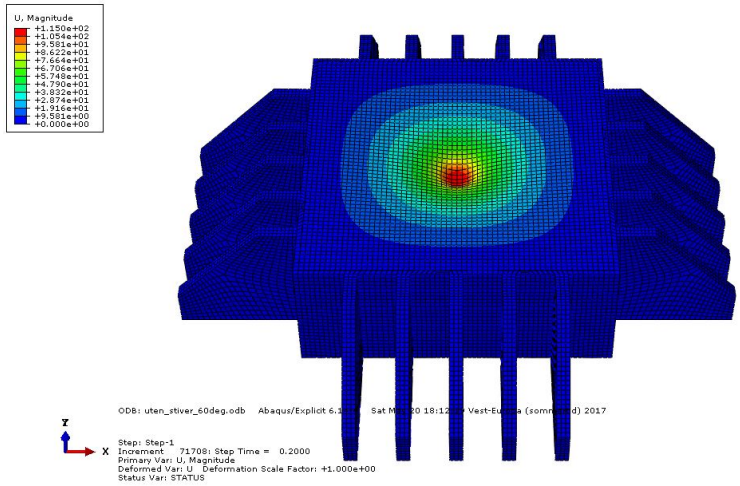

Figure C.4: The displacement pattern for the unstiffened plate at -60°C using the Nam material.

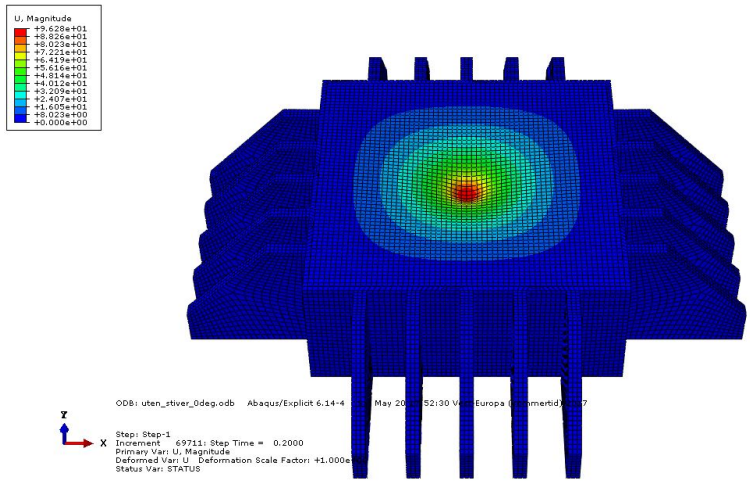

Figure C.5: The displacement pattern for the unstiffened plate at room temperature using the Nam material.

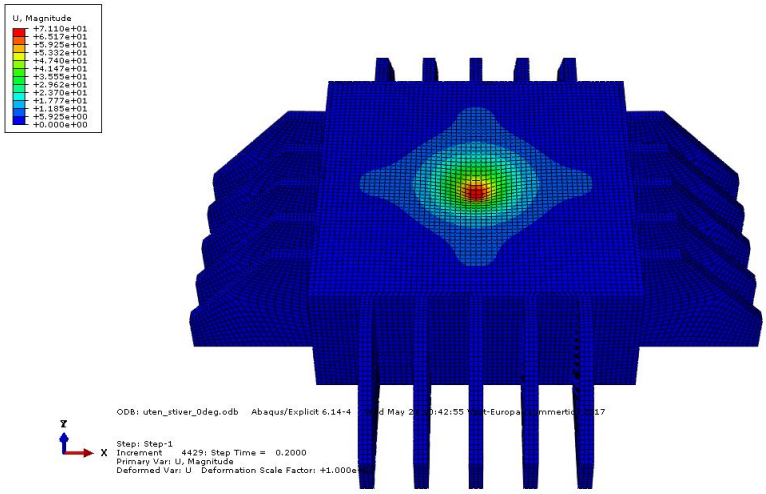

Figure C.6: The displacement pattern for the unstiffened plate at room temperature using the paik material.

Appendix D

Additional figures from the ship side impact

This chapter contains additional figures showing the damage to the ship hull after impact at different temperatures. The deformation has not been scaled at any of the following figures.

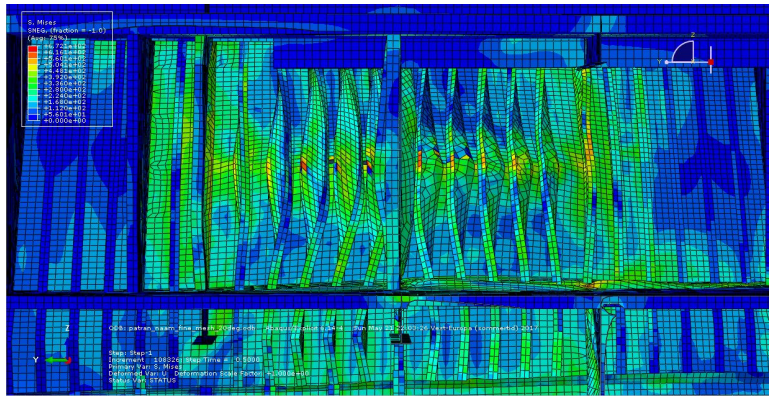

Figure D.1: The damaged area of the hull after impact at room temperature.

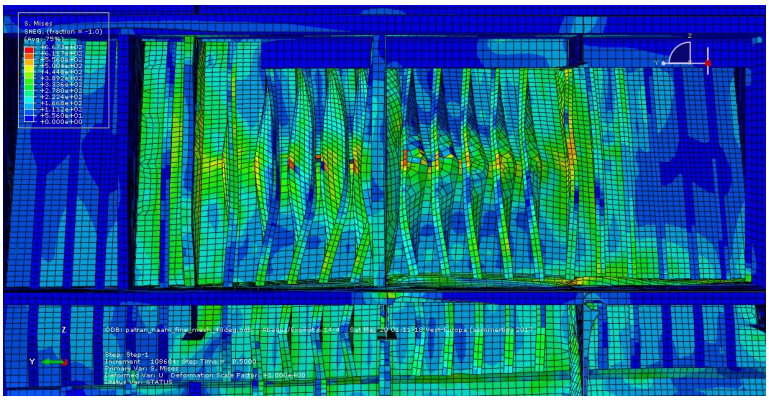

Figure D.2: The damaged area of the hull after impact at -40°C.

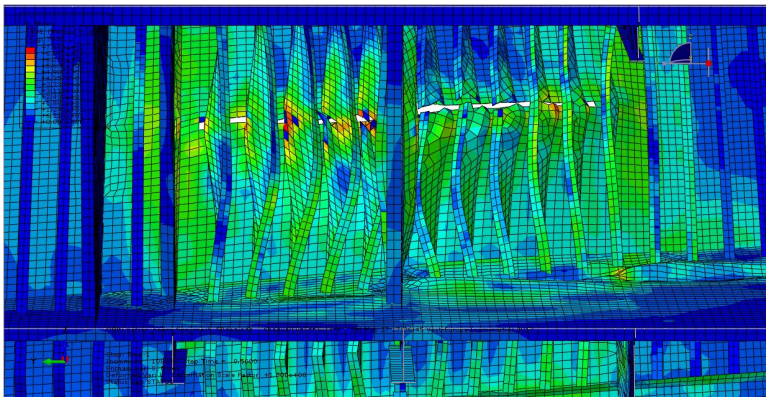

Figure D.3: The damaged area of the hull after impact at -50°C.

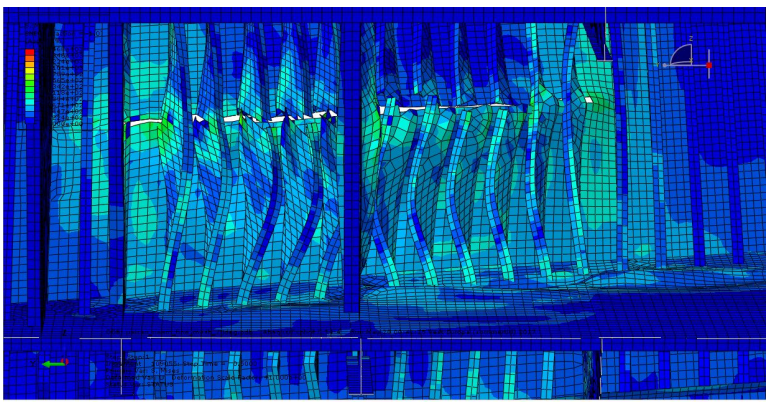

Figure D.4: The damaged area of the hull after impact at -70°C.

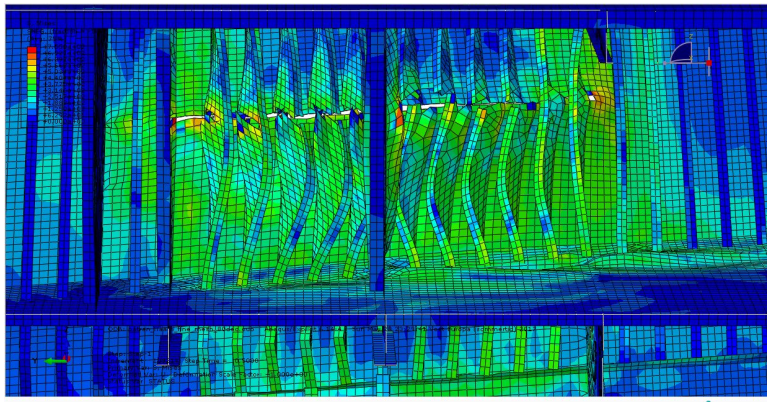

Figure D.5: The damaged area of the hull after impact at -80°C.

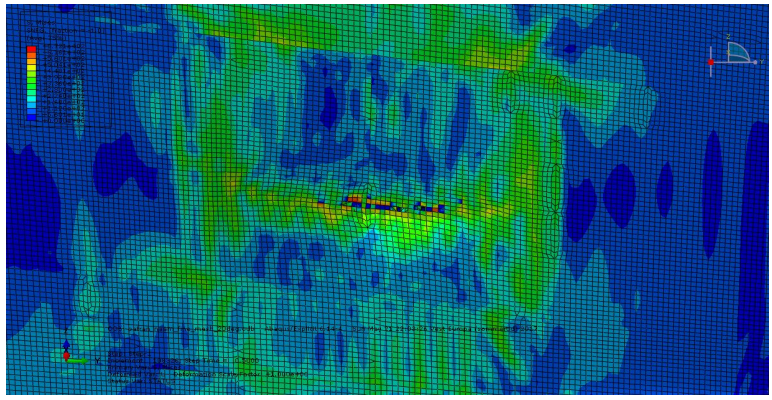

Figure D.6: The hull side of the damaged area of the hull after impact at room temperature.

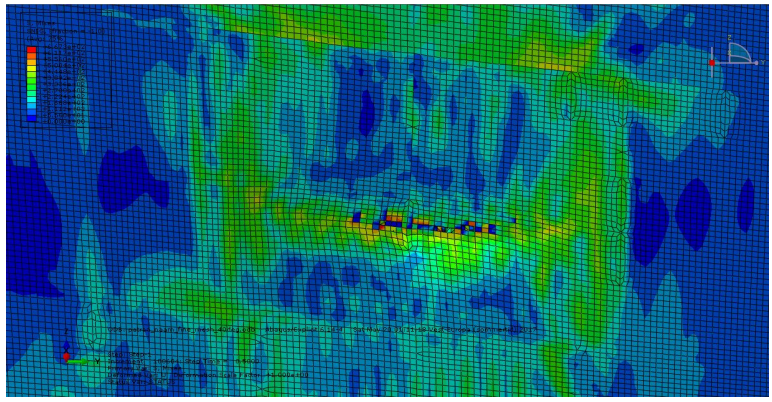

Figure D.7: The hull side of the damaged area of the hull after impact at -40°C.

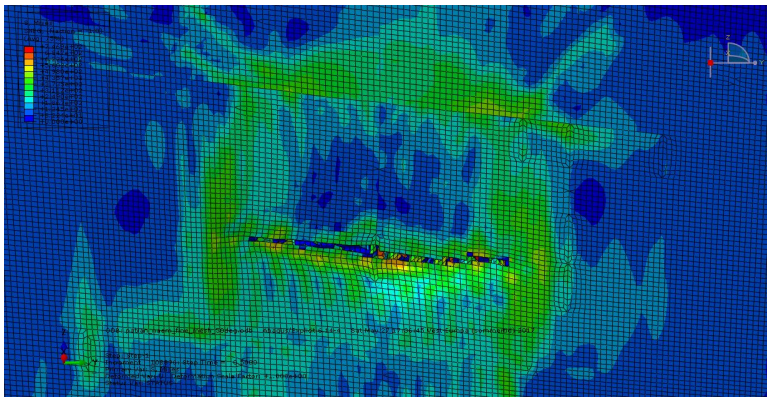

Figure D.8: The hull side of the damaged area of the hull after impact at -50°C.

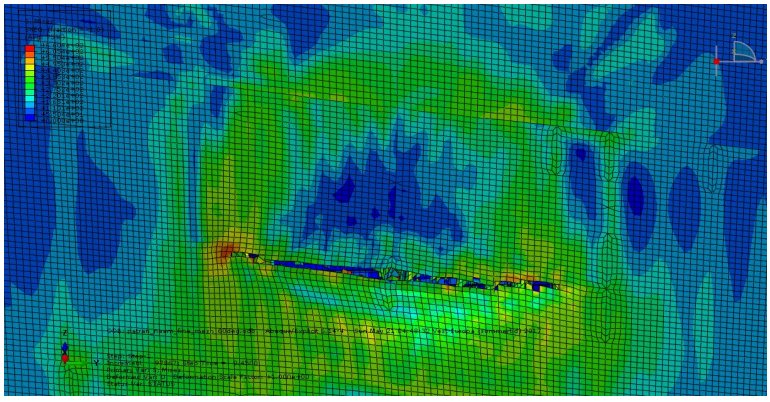

Figure D.9: The hull side of the damaged area of the hull after impact at -60°C.

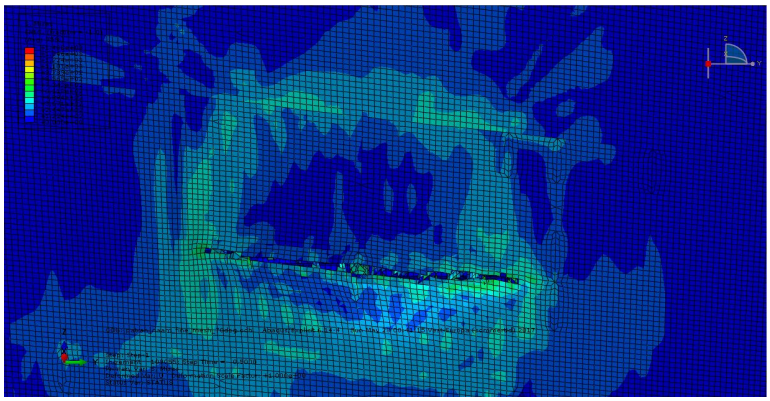

Figure D.10: The hull side of the damaged area of the hull after impact at -70°C.

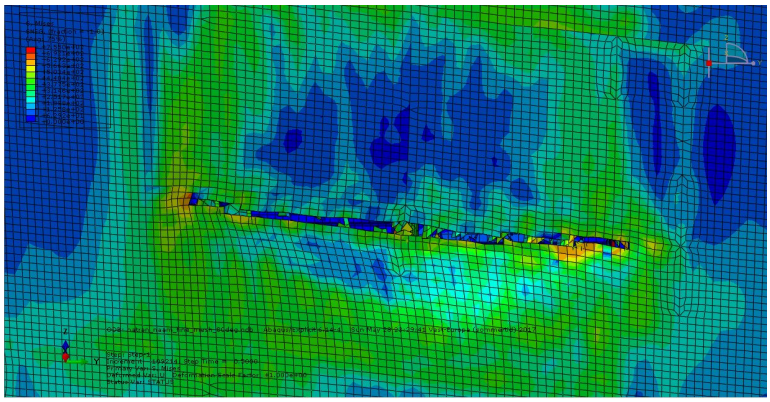

Figure D.11: The hull side of the damaged area of the hull after impact at -80°C.

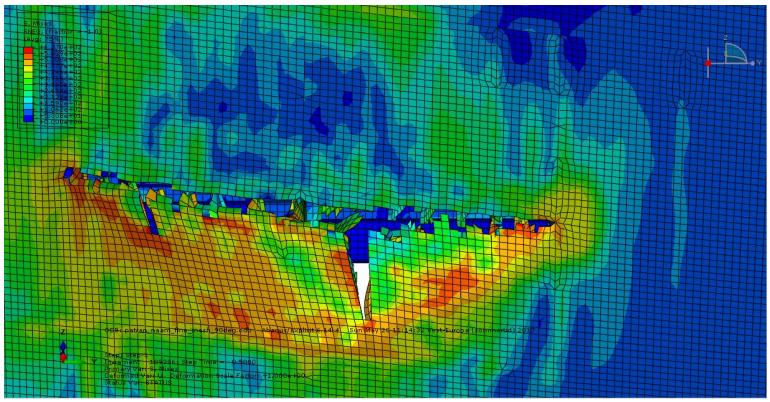

Figure D.12: The hull side of the damaged area of the hull after impact at -90°C.

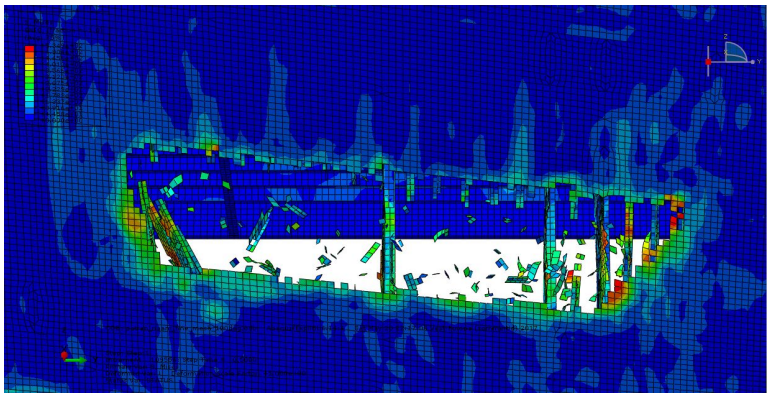

Figure D.13: The hull side of the damaged area of the hull after impact at -100°C.